minerals

MDPI

Article

Diagenesis and the Conditions of Deposition of the Middle Jurassic Siderite Rocks from the Northern Margin of the Holy Cross Mountains (Poland)

Aleksandra Kozłowska [1,*], Anna Feldman-Olszewska [1], Marta Kuberska [1] and Anna Maliszewska [2]

[1] Polish Geological Institute-National Research Institute, Rakowiecka 4, 00-975 Warsaw, Poland; anna.feldman-olszewska@pgi.gov.pl (A.F.-O.); marta.kuberska@pgi.gov.pl (M.K.)
[2] Retired Employee of Polish Geological Institute-National Research Institute, Rakowiecka 4, 00-975 Warsaw, Poland; anna.maliszewska74@gmail.com
* Correspondence: aleksandra.kozlowska@pgi.gov.pl

Abstract: The aim of the present study is to reconstruct sedimentary conditions of Middle Jurassic rocks that contain siderites to identify the mineral composition of the inserbeds and to recognize the origin of the siderite. Thin inserbeds of siderite rocks occur most frequently within Bajocian siliciclastic deposits and, more rarely, Aalenian and Bathonian. The research material comes from 11 boreholes located in the north and northeastern margins of the Holy Cross Mountains. The research methods included sedimentological analyses, and studies in polarizing and scanning electron microscopes, staining of carbonates, cathodoluminescence, X-ray structural analysis, and stable carbon and oxygen isotopic determinations were used. Middle Jurassic sideritic rocks are most often represented by clayey siderites, which also include muddy and sandy varieties and siderite sandstones. There are also local occurrences of coquinas, claystones, mudstones, and siderite conglomerates. The main component of sideritic rocks is sideroplesite. Berthierine, pistomesite, calcite, and ankerite are important components, too. The action of diagenetic processes of cementation, compaction, replacement, and alteration within the Middle Jurassic deposits was most intense during the eo- and mesodiagenesis. The sedimentological analysis showed that most of the studied siderites were formed in a low-oxygenated marine environment, mainly in the transition zone between the normal and storm wave bases and in the lower and middle shoreface zones. The results of the petrographic, mineralogical, and geochemical studies indicated the origin of the sideritic rocks mainly in the marine environment, with the participation of meteoric water. There were slight differences in the chemical composition of sideroplesite depending on the environment it crystallized in. There was no correlation between the values of the carbon isotope determinations in the sideroplesite and the environmental conditions of its crystallization. Slight differences were visible in the case of the average values of $\delta^{18}O$ in the sideroplesite.

Keywords: sideritic rocks; diagenesis; sedimentology; Middle Jurassic; Holy Cross Mountains

Citation: Kozłowska, A.; Feldman-Olszewska, A.; Kuberska, M.; Maliszewska, A. Diagenesis and the Conditions of Deposition of the Middle Jurassic Siderite Rocks from the Northern Margin of the Holy Cross Mountains (Poland). *Minerals* **2021**, *11*, 1353. https://doi.org/10.3390/min11121353

Academic Editor: Luca Aldega

Received: 2 November 2021
Accepted: 26 November 2021
Published: 30 November 2021

1. Introduction

Research on the Middle Jurassic siderite iron ores in the northern margin of the Holy Cross Mountains was initiated by Kuźniar [1,2]. His most extensive publication concerned the siderite iron ore deposit in Parczów [3], the exploitation of which started in the 1920s. However, the initiated siderite research was abandoned, because the production of ores appeared unprofitable. In the 1920s, research on iron deposits was also carried out and continued after World War II in the Częstochowa region [4,5]. In the Łęczyca region, Kujawy and Znosko [6,7] documented an iron ore deposit composed of sideritic coquinas. However, the iron content of the siderites turned out to be too low for extraction.

The first systematic studies on the stratigraphy and ore potential of Middle Jurassic rocks in the northeastern margin of the Holy Cross Mountains were conducted in the 1930s

and 1940s by Różycki [8,9]. In the northern margin, regional research was carried out by Karaszewski [10] and Cieśla [11,12]. Stratigraphic–lithological sections and correlations of boreholes drilled in the late 1950s by the Geological Institute in the Sady-Omięcin-Jastrząb area were presented by Daniec [13]. A summary of the knowledge on the lithologies and stratigraphy of Middle Jurassic deposits in the Holy Cross Mountains margin was provided by Daniec [14].

Petrographic studies of iron ores in Poland are known from the 1960s. In 1961, Turnau-Morawska [15] characterized the Lower Bathonian ore-bearing formations in the Łęczyca region, Kujawy. That author also made a comparison of the Łęczyca siderites with those from the deposits in the Parczów and Częstochowa regions. In 1963 and 1964, Dadlez [16,17] presented petrographic characteristics of Middle Jurassic iron ores from the Kamień Pomorski region. In 1966, Ekiert [18] published a petrographic study of Doggerian iron deposits from the Częstochowa region. Mineralogical studies of siderite interbeds in Middle Jurassic siliciclastic rocks from the Polish Lowlands were conducted by Maliszewska [19] and Maliszewska et al. [20–23]. Kozłowska's studies provided petrographic analyses of siderite rocks from the northeastern margin of the Holy Cross Mountains [24–30] and the Częstochowa region [26,28–31].

Information on sedimentary conditions of siderite rocks can be found in studies of ore-bearing clays from the Częstochowa region (e.g., References [32–36]). In recent years, Feldman-Olszewska [26,31] and Leonowicz [37–40] conducted sedimentological analyses of Middle Jurassic deposits in the Częstochowa region. Single publications contain sedimentological data on rocks containing Middle Jurassic siderite interbeds in the northeastern margin of the Holy Cross Mountains [25].

Among the cited literature, there is no publication that would contain the results of both petrographic and sedimentological studies. In foreign literature, you can find publications that combine sedimentological research with the genesis of siderite (e.g., References [41–43]). Our contribution aims at presenting integrated results of sedimentological analyses of rocks that contain siderites and their petrographic studies. Previously, such studies were not done in Poland. Our results allowed reconstructing sedimentary conditions of Middle Jurassic rocks that contain siderites, in the N and NE margin of the Holy Cross Mountains, to identify the mineral compositions of the inserbeds and to recognize the origin of the siderite. Thin inserbeds of siderite rocks occur most frequently within the Bajocian siliciclastic deposits, more rarely Aalenian and Bathonian.

2. Geological Setting

The Holy Cross Mountains are massifs built of Palaeozoic rocks folded at the passive margin of Baltica during Variscian movements [44]. They consist of two units: the Łysogóry Unit and Kielce Unit separated by the Holy Cross Fault [45–47]. In Permian and Mesozoic times, the Holy Cross area was a part of epikontinental Germanic-Polish Basin, and the development of sedimentation in the study area in that times should be considered in terms of the history of development of the Mid-Polish Trough—more specifically, its SE part [48]. Mid-Polish Trough was a geologic structure connected with the Teisseyre-Tornquist zone that developed at the edge of the East European Craton in the Alpine stress field that caused an oblique extension [49,50]. In Permian and Mesozoic times, the Holy Cross area was covered by a few kilometers-thick marine and continental deopsits [51]. Tectonic movements of the Laramide phase reactivated the Variscian fault system, caused an elevation of the Holy Cross area, and removed the Permian and Mesozoic deposits [49,52].

The Paleozoic core of the Holy Cross Mountains is surrounded on the southwest, north, and northeast by Mesozoic formations, the so-called Mesozoic margin composed of Triassic and Jurassic deposits. Its boundary is marked by the outcrops of Paleozoic rocks in the Holy Cross region. Lying at the boundary of tectonic units that ultimately formed at the end of the Alpine orogeny, the northern area of the Mesozoic margin is part of the Gielniów segment of the Holy Cross Swell [53], whereas its northeastern area is part of the transition zone from the Mid-Polish Swell to the Marginal Trough [54,55]. As we move

away from the boundary of the Paleozoic outcrops, younger and younger Triassic rocks and then successively younger and younger Lower, Middle, and Upper Jurassic formations appear under the Cenozoic [56].

In the area of the fully developed Middle Jurassic section (Aalenian to Callovian), its thickness is varied in the boreholes studied (Figure 1): in the Wąglany k/Opoczna (the designation, Wąglany will be used in the following part of the publication)—449.0 m, in the Władysław—376.0 m, Mniszków IG 1—302.5 m, Mołdawa—448.6 m, and Wyszmontów 1—163.9 m [13,14]. In the Gutwin borehole, it is impossible to establish accurately the lower boundary of the Middle Jurassic, as it falls within a 30-meter-thick non-cored section (between 312 m and 344 m in depth). The thickness of the Middle Jurassic in this borehole is between 264.5 m and 296.5 m. In the remaining boreholes, the Middle Jurassic section is incomplete. The most complete one was found in the Omięcin XI/3 borehole, in which the uppermost Middle Jurassic (Callovian) and the top part of the Upper Bathonian were the only missing intervals. These deposits were removed during inversion of the Mid-Polish Trough. A similar erosional gap can be observed in the Omięcin XI/2 borehole, in which the youngest Middle Jurassic deposits, found directly under the Quaternary, represent the Upper Bajocian. The thicknesses of the Jurassic sections in both boreholes are 221.8 m and 215.7 m, respectively; however, at the present stage of stratigraphic knowledge, it cannot be clearly stated whether only the Middle Jurassic or also the uppermost Lower Jurassic are present in the lowest part of the borehole sections. In the Zalesie Antoniowskie 1 borehole, the Aalenian–Bajocian section is 110.0 m thick. Only small parts of the section were drilled in the remaining two boreholes, which probably represent the Upper Bajocian. In the Justynów PIG 1 borehole (9.5 m), they overlie claystones of the Lower Jurassic Ciechocinek Formation. In the Wyszmontów PIG 2 borehole, 40.0-m-thick Jurassic deposits, which were drilled directly under the Quaternary, represent the Upper Bajocian.

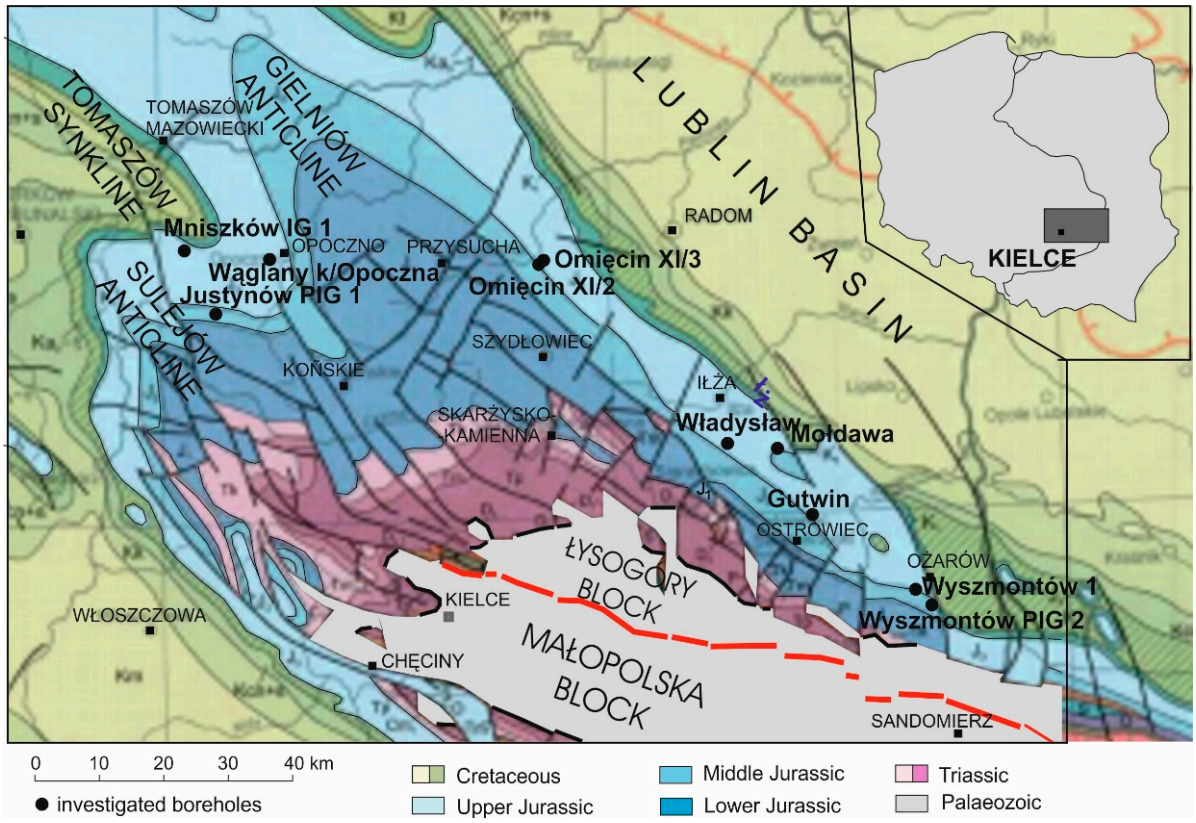

Figure 1. Location of boreholes on the background of the geological map without Cainozoic deposits (after Reference [56]).

3. Materials and Research Methods

The research material comes from 11 boreholes located in the northeastern margin of the Holy Cross Mountains: Gutwin, Justynów PIG 1, Mniszków IG 1, Mołdawa, Omięcin XI/2, Omięcin XI/3, Wąglany, Władysław, Wyszmontów 1, Wyszmontów PIG 2, and Zalesie Antoniowskie (Figure 1). Most of them (Gutwin, Mołdawa, Omięcin XI/2, Omięcin XI/3, Wąglany, Władysław, Wyszmontów 1, and Zalesie Antoniowskie) are historical fully cored boreholes drilled in the 1950s and 1960s, in which no well-log measurements were made. The core recovery in these boreholes was below 100%; however, it was good enough to identify the lithological succession. The poorest core recovery was reported from both boreholes drilled in the Omięcin region. The remaining three boreholes were drilled in the 1980s. The Justynów PIG 1 and Wyszmontów PIG 2 boreholes were completely cored shallow mapping wells, and the only deep borehole—Mniszków IG 1 [57], with borehole geophysics documentation—was cored fragmentarily. In the Zalesie Antoniowskie borehole, sedimentological studies were performed only for the lowest 20-m section of Middle Jurassic deposits, due to the lack of preserved drill core material.

In order to determine sedimentary environments of the Middle Jurassic deposits, the available drill core and well-log material was analyzed. A detailed sedimentological analysis of drill cores was performed for all the wells discussed, enabling the identification of a number of lithofacies. The following features were examined: rock lithology; thickness; characteristics of the base and top boundaries; grain size; color; cement type; original sedimentary structures; additional lithological constituents (presence of clasts, pebbles, siderites, and coals); presence of flora and fauna fossil remains; trace fossils; and the degree of sediment bioturbation. If possible, a taxonomic identification of the types of trace fossils was performed. The lithofacies distinguished were classified using standard lithofacies codes introduced by Farrell et al. [58] and supplemented by Zieliński and Pisarska-Jamroży [59], though slightly modified. Based on the vertical lithofacies sequence, sedimentary cycles have been identified in the individual sections.

Each cycle begins at the base and ends at the top by an erosional or sharp lithological boundary; within the cycle, the transitions between lithofacies are gradual. The only exceptions are interbeds of storm origin, a few centimeters in thickness, which is at least an order of magnitude smaller than the thickness of the identified cycles. The interpretation of sedimentary environments was performed based on rich sedimentological literature, including References [60–66]. The interpretation of the sedimentary environments was also based on the results of the analysis of the sedimentary environments of the Middle Jurassic deposits in the Kujawy region (References [67–75] and the literature cited therein).

The archived and published results of the microfossil analyses of Kopik and the determinations of the ammonites by Deczkowski [13,14] for the analyzed boreholes were used. In addition, information on the Middle Jurassic stratigraphy provided in the papers by Różycki [9], Cieśla [11], Dayczak-Calikowska and Kopik [76], and Dayczak-Calikowska [77] was also used for proper correlation of boreholes. Additionally, a regional correlation with the complex of Middle Jurassic rocks of the adjacent Radom-Lublin region [78,79] was adopted. Based on the interpretation of sedimentary environments and all collected litho- and biostratigraphic data, a correlation cross-section was constructed across the boreholes analyzed in this study.

A microscopic analysis of 156 thin sections was performed on a Nikon Optiphot 2 polarizing microscope (Japan). The percentage content (vol.%) of the mineral composition of the siderite rocks was obtained from a planimetric analysis using the point method, counting up to 300 grains. All thin sections were stained with Evamy's solution to determine the type of carbonate cements. Thirty-five samples of siderite rocks were subjected to cathodoluminescence (CL) analysis. The examinations were carried out on an English device of the so-called cold cathode, model CCL 8200 mk 3 by Cambridge Image Technology Ltd (Great Britain), mounted on a Nikon polarizing microscope. Scanning electron microscopy (SEM) examinations were performed with the use of two microscopes: JSM-35 type from JEOL (Japan) and LEO 1430 type, equipped with Oxford Instruments EDS

ISIS energy microprobes (SwitzerlandThirty-five preparations were analyzed; these were uncovered, polished, and carbon-sputtered sections. One hundred and thirty-seven quantitative analyses of carbonates were performed and converted to molecular compositions. SEM Quant software (Great Britain) was used for the X-ray quantitative analysis when examining micro areas. Fluid inclusion studies were performed on two-sided polished preparations using the Linkam THMS600 heating and freezing stages mounted on a Nikon Eclipse LV100 Pol polarizing microscope (Japan, see References [29,30]). X-ray investigations of selected samples were carried out on an X'Pert PW 3020 X-ray diffractometer from Philips Company (Enschede, The Netherlands) (see Reference [28]). Isotope studies of oxygen and carbon in carbonate cements were performed on 56 rock samples at the Mass Spectrometry Laboratory of the Institute of Physics, Maria Curie-Skłodowska University in Lublin. Fifty-three of them were analyzed for siderite, and three samples were examined for calcite. The determinations were made mainly on clay siderites and siderite sandstones, in which iron carbonate was represented exclusively or almost exclusively by finely crystalline sideroplesite and siderite. Moreover, two samples containing rhombohedral crystals of pistomesite and sideroplesite were examined. Studies of the isotopic compositions of oxygen and carbon were carried out on gaseous CO_2 obtained from carbonate samples according to the standard procedures for the reaction with phosphate acid [80,81]. The measurements were made on a modified MI1305 spectrometer [82–85]. The accuracy of the measurements was ±0.1‰.

4. Results

4.1. Sedimentological Analysis—Lithofacies Characteristics and Cyclicity

Twenty-three lithofacies were distinguished in the analyzed Middle Jurassic sections. Their summaries, characteristics, and interpretation of the deposition mechanisms are presented in Table 1. Based on the vertical sequences of the lithofacies, several types of sedimentary cycles were distinguished in the sections: coarsening-upward, fining-upward, and non-gradational cycles comprising both clastic and carbonate rocks. The sequences of the lithofacies in the individual cycles and their stratigraphic positions are shown in Figure 2A–G.

Table 1. Characteristics of the lithofacies present in the investigated cores.

Code of Lithofacies after [58,59] Modified	Lithofacies	Main Features	Color	Deposition Mechanism
GB	Medium- or pour sorted conglomerates	lack of bedding	grey, brown	erosional surface or deposition in upper plane bed (upper regime flow)
M_m	Massive claystones and shales	lack of bedding, cleavage	dark grey	deposition of clay from suspension in very calm marine environment
M_{lam}	Claystones and shales with single 1 mm thick lenses of silt	lenticular lamination	dark grey	deposition from suspension alternately with rare deposition by low-density currents of very low velocity
T_m TS_m	Massive mudstones and sandy mudstones	massive	dark grey	deposition of mud and silt from suspension
T_{biot}	Completely bioturbated mudstones	very strong bioturbation up to total obliteration of sedimentary structures	dark grey, grey	deposition of mud from suspension, strong bioturbation by bottom fauna during the slowing down the rate of sedimentation or improvement of degree of oxygenation of the bottom water
$H_{F>S1}$	Lenticular laminated mudy heteroliths with flat, elongated lenses of sand	lenticular lamination	dark grey/light grey	alternately deposition of mud from suspension in condition of lack of water movement and deposition from currents poor in sand; predominance of quiet periods
$H_{F>S2}$	Lenticular bedded mudy heteroliths with thick lenses of sand	lenticular bedding	dark grey/light grey	alternately deposition of mud from suspension in condition of lack of water movement and deposition from currents richer in sand; predominance of quiet periods

Table 1. *Cont.*

Code of Lithofacies after [58,59] Modified	Lithofacies	Main Features	Color	Deposition Mechanism
$H_{F=S}$	Heteroliths with equal proportion of mud and sand	lenticular and wavy bedding	dark grey/light grey	alternately deposition of mud from suspension in condition of lack of water movement and deposition from currents rich in sand
S_w	Wavy-bedded sandstones	wavy bedding	light grey/dark grey	deposition of sand from weak traction currents alternately with deposition of mud from suspension in condition of lack of water movement; predominance of sand deposition
S_f	Flaser-bedded sandstones	flaser bedding	light grey	deposition of sand from weak traction currents alternately with deposition of mud from suspension in condition of lack of water movement; erosion of ripple marks ridges
S_{lam}	Sandstones with clay laminae	single horizontal or wavy clay laminae	light grey or grey	deposition of sand from strong traction currents alternately with rare deposition of mud from suspension
S_b	Sandstones with clay or mud beds	horizontal intercalations	light grey or grey	deposition of sand from strong traction currents alternately with less frequent deposition of mud from suspension
S_m	Massive sandstones	massive	light grey or grey	fast deposition from sharply decelerating density currents; mass deposition from highly concentrated gravity flows; deposition from traction currents in upper flow regime (antidunes); or obliteration of sedimentary structures as a result of sediment liquefaction
S_l	Horizontally laminated sandstones	horizontal lamination	light grey	deposition from traction currents in "upper plane bed phase"
S_{xt}	Tabular cross-bedded sandstone	tabular cross-bedding	light grey	deposition from strong traction currents in "lower plane bed phase" (migration of sand dunes)
S_{xl}	Low-angle cross-bedded sandstones	low-angle cross-bedding	light grey	deposition from oscillatory flows caused by big storm waves and complex flows (HCS, SCS) or deposition from traction currents in upper regime flow (antidunes)
S_r	Ripple-bedded sandstones	ripple-bedding	light grey	deposition from weak traction currents in "lower plane bed phase" (low flow regime) or deposition from oscillatory flows of low velocity
S_{xi}	Trough (large-scale) cross-bedded sandstone	trough (large-scale) cross bedding	light grey or grey	deposition from strong traction currents in "lower plane bed phase" (low flow regime) (large ripple marks)
S_{Fe}	Chamosite sandstones	massive or cross-bedding (tabular or trough); chamosite in cement	green-grey or green	deposition from traction currents in nearshore and tidal flats, near river mouth, in weakly reduction environments, in warm and humid climate
S/L	Calcareous sandstones, sandy limestones	massive	light grey	deposition on the siliciclastic-calcareous shelf from sharply decelerating density currents or from traction currents in upper flow regime (antidunes)
L	Crinoidal and marly limestones	pakstones or wakstones	rusty, light brown, light grey	sedimentation in situ on the middle ramp
D	Sandy dolomites	massive	grey	dolomite cementation

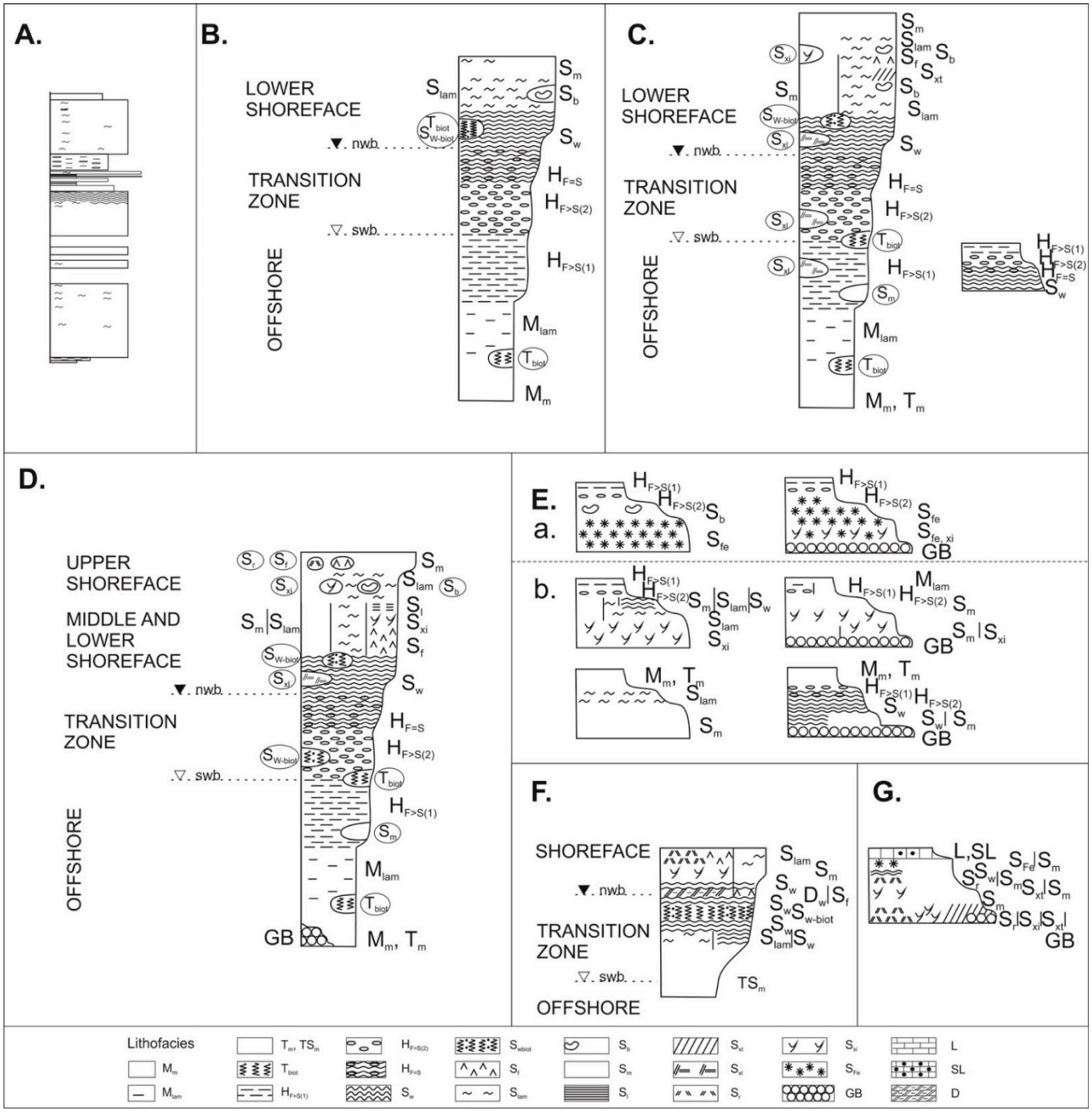

Figure 2. Vertical sequences of lithofacies observed in different stratigraphic divisions: (**A**) exemplary profile of the Lower Aalenian, (**B**) Upper Aalenian–Lower Bajocian, (**C**) Upper Bajocian, (**D**) Lower and Middle Bathonian—coarsening-up cycles, (**E**) Lower and Middle Bathonian—finning-up cycles; (**a**). cycles with green colour chamosite sandstones (lithofacies SFe), (**b**). cycles without green colour chamosite sandstones (lithofacies SFe), (**F**) Upper Bathonian–Callovian—coarsening-up cycles, and (**G**). Upper Bathonian–Callovian—finning-up cycles. Symbols of lithofacies and their descriptions are as in Table 1. nwb—normal wave base; swb—storm wave base; SFe—Fe.

4.1.1. Aalenian

In all of the boreholes, the Lower Aalenian is composed predominantly of fine-grained sandstones representing mainly S_m, and S_{lam} lithofacies, less often S_f or S_w, and, in the Wyszmontów 1 borehole, also S_{xl} (an exemplary section is presented in Figure 2A). They

contain muscovite, kaolinite, coal fragments, and clay clasts. The laminae in sandstone are often carbonaceous. Among trace fossils, it was possible to identify *Palaeophycus* isp. and *Skolithos* isp. in the Wąglany borehole, *Diplocraterion* isp. in the Mołdawa borehole, and *Planolites beverleyensis* (Billings) in the Władysław borehole.

The middle part of the Wąglany borehole (depth 607.0–612.5 m) is represented by sandy mudstones (TS lithofacies) with a few levels of siderites and siderite concretions. They contain bivalves and pyritized plant detritus. Sideritized mudstones and sandstones, probably corresponding to the Aalenian ore-bearing level [13,14], were also found in the Omięcin XI/2 and XI/3 boreholes. In the Omięcin XI/3 borehole, at a depth of 228.3 m, there is a conglomerate level (GB lithofacies), at the base of which the boundary between the Lower and Middle Jurassic is drawn.

Muddy clay deposits usually appear occasionally and are represented by lithofacies M_m and T_m (Wąglany and Gutwin) and M_{lam} (Mołdawa). In the Mołdawa borehole, *Planolites* isp. and *Chondrites* isp. trace fossils, and a few centimeters-thick interbed of clayey siderite were found in these deposits. A complex of laminated heteroliths (lithofacies $H_{f>s1}$) with fragments of coalified flora was identified only in the Wyszmontów 1 borehole.

4.1.2. Upper Aalenian

The Upper Aalenian is composed mainly of black noncalcareous clay shales (M_m and M_{lam} lithofacies) with pyritized plant detritus, trace fossils of *Chondrites* isp., less frequent *Planolites* isp., and scarce marly-sideritic concretions (Gutwin and Władysław) (Figure 2B). Subordinate mudstone facies (lithofacies T_m, TS, and T_{biot}) occur in the Władysław and Zalesie Antoniowskie boreholes, and heteroliths are found in the Omięcin region (lithofacies $H_{f>s1}$ and $H_{f>s2}$).

4.1.3. Lower Bajocian

The Lower Bajocian section is a continuation of the Upper Aalenian sedimentation (Figure 2B). In the analyzed boreholes, it shows some lithofacial differentiation; however, the common feature is a coarsening-upward trend.

The Mid-Polish Trough's most typical lithological section is observed in the Wyszmontów 1 borehole. It is represented by a coarsening-upward cycle of the following lithofacies succession: $M_{lam} \rightarrow H_{f>s2} \rightarrow H_{f=s} \rightarrow S_w$. Trace fossils: *Planolites* isp. and *Chondrites targioni* Brongniart are relatively frequent in the claystones and heteroliths, while abundant muscovite occurs in the sandstones.

In the Wąglany borehole, the lower part of the section is made up of clayey deposits representing lithofacies M_m, while the upper part is composed of fine-grained sandstones of lithofacies S_w, S_m, and S_{lam}.

The Władysław borehole section is dominated by fine-grained deposits of the lithofacies succession $M_m \rightarrow M_{lam} \rightarrow H_{f>s1} \rightarrow TS_m \rightarrow S_m$. The silt/clay heteroliths are slightly bioturbated by *Chondrites targioni* Brongniart and contain bivalve fossils and siderite concretions.

A similar section, represented by the lithofacies succession $M_m \rightarrow M_{lam} \rightarrow T_{biot}$, is found in the nearby Gutwin borehole. The clay facies contain infrequent siderite concretions, while the mudstones show complete bioturbation by *Chondrites targioni* Brongniart.

In the Omięcin XI/2 and Omięcin XI/3 boreholes, the Lower Bajocian is probably reduced and is composed mainly of heteroliths ($H_{f>s2}$). There are also fine-grained sandstones with an admixture of medium grains (lithofacies S_m and S_{lam}), which are found in the upper part of the section.

The drill core yield from the Lower Bajocian section in the Mołdawa borehole is relatively poor. Highly bioturbated deposits dominate the core material obtained: fine-grained sandstones with an admixture of medium grains and mudstones. *Chondrites targioni* Brongniart, *Planolites* isp., and *Bergaueria* isp. were found in these deposits. In contrast to the other sections, the lithofacies are often arranged in fining-upward cycles ($S_{wbiot} \rightarrow TS_{biot} \rightarrow T_{biot}$). Muscovite

and coalified plant detritus are observed rarely. There is a slight sideritization at the top of the section.

4.1.4. Upper Bajocian

In the lowermost part of the Upper Bajocian in the Władysław borehole, $H_{f>s1}$ is the dominant lithofacies type. In the remaining boreholes, sandstones occur, representing lithofacies S_w, S_m, or S_{lam} with muscovite and occasional trace fossils of *Chondrites* isp., *Planolites* isp., and *Planolites beverleyensis* (Billings).

The remaining part of the Upper Bajocian section is represented by one to six coarsening-upward sedimentary cycles of different thicknesses (Figure 2C). Each cycle begins with clay shales or claystones representing lithofacies M_m or M_{lam}. The deposits contain relatively numerous trace fossils: *Chondrites targioni* Brongniart (in places resulting in complete bioturbation of the sediment—intercalations of lithofacies T_{biot}), *Planolites* isp., and *Planolites beverleyensis* (Billings). In addition, *Schaubcylindrichnus* isp. was found in the Wąglany and Mołdawa boreholes, while, in the Omięcin XI/3 borehole, *Gyrochorte comosa* Heer was identified. Muscovite, bivalve fossils, and microfossils are present in the rock, and there is abundant pyritized plant detritus. In the Mołdawa borehole, siderite concretions are also frequent, while, in the Wyszmontów 1 borehole, a clay siderite interbed is found at a depth of 129.1–129.6 m.

Towards the top of each sedimentary cycle, we observed a gradual increase in the admixture of sand material, expressed as a lithofacies succession of $M_{lam} \rightarrow H_{f>s1} \rightarrow H_{f>s2} \rightarrow H_{f=s} \rightarrow S_w$ (Figure 2C). Interbeds of sandstones of lithofacies S_{xl}, bounded at the base by sharp boundaries, were rare in these lithofacies. In the upper parts of the cycles, fine-grained sandstones representing lithofacies S_m and S_{lam} (containing abundant muscovite) were the most common. In the Wąglany borehole, a thin layer of lithofacies S_{xt} was also identified. Moreover, there were medium- and coarse-grained sandstones of lithofacies S_{xi} in the uppermost parts of the cycles in the Mołdawa borehole.

The Upper Bajocian section contained siderite deposits in the form of interbeds and lenses in mudstones and irregular sideritization in sandstones.

4.1.5. Lower and Middle Bathonian

In the study boreholes, the Lower and Middle Bathonian section is highly diverse in terms of both thickness and facies. The characteristic feature is the presence of frequent conglomerate layers in the bottom portions of sedimentary cycles and the occurrence of highly bioturbated deposits, both mudstones and sandstones. However, the layers are not observed in the axial zone of the Middle Jurassic sedimentary basin (Wąglany borehole).

In the individual boreholes, four to five coarsening-upward sedimentary cycles were found (Figure 2D). Moreover, in the Mołdawa and Władysław boreholes, several additional fining-upward cycles are present in the upper part of the section (Figure 2E).

Particular cycles start either with conglomerate levels (lithofacies GB, several to tens of centimeters thick) passing into claystones, or there are claystone facies from the very base. In the lower part of the cycles, a lithofacies succession of $M_{lam} \rightarrow H_{f>s1} \rightarrow H_{f>s2} \rightarrow H_{f=s} \rightarrow S_w$ is observed. In the Gutwin—Wyszmontów region, some parts of the section are intensely bioturbated (lithofacies T_{biot} and S_{wbiot}) with *Planolites* isp., *Planolites beverleyensis* (Billings), *Chondrites targioni* Brogniart, and a single *Thalassinoides* isp. Thin interlayers of sandstone lithofacies S_m and S_{xl} are observed occasionally. A characteristic feature of the lower parts of the cycles is the frequent presence of muscovite and the occurrence of numerous bivalves, locally forming coquina levels.

The upper parts of the cycles are represented mainly by fine-grained sandstones, with occasional medium-grained ones at the top, which show different lithofacies successions. The following associations are identified here: $S_w \rightarrow S_m \rightarrow S_{xi} \rightarrow S_m$; $S_w \rightarrow S_{lam} \rightarrow S_{xl} \rightarrow S_m$; $S_w \rightarrow S_{lam}$; $S_w \rightarrow S_f \rightarrow S_{xi} \rightarrow S_l \rightarrow S_{lam} \rightarrow S_m$ (Figure 2D). The medium-grained sandstones also contain interbeds of lithofacies S_r and S_f. Moreover, a direct transition of mudstones into lithofacies S_{xl} is observed in the lower cycles of the Gutwin

and Wyszmontów 1 boreholes. Trace fossils are rare in the sandstones, and *Skolithos* isp., *Palaeophycus* isp., and *Ophiomorpha* isp. occasionally occur. In the Omięcin XI/3 and Gutwin boreholes, the upper and middle sections of the cycles contain grey–green chlorite sandstones above the mudstones and, occasionally, also iron ooids.

In all the sections, siderite intercalations and sideritization of the entire rock are quite common in both mudstones and wavy-laminated sandstones. The occurrences of siderites are particularly numerous in the lower part of the Bathonian section.

As mentioned above, fining-upward cycles were identified in the upper part of the Middle Bathonian in the Mołdawa and Władysław boreholes (Figure 2E). At the bottom of the cycle, there is a conglomerate level (lithofacies GB) or an erosional boundary, overlain by coarse-grained sandstones followed by medium- to fine-grained ones. The sandstones often differ from those described above. These are grey–green chlorite sandstones cemented with clay cement (lithofacies S_{Fe}) showing a massive structure or trough cross-bedding. Locally, they contain muscovite. In the upper cycles of the Mołdawa borehole, there are numerous clay clasts and small sandstone pebbles with limonite rims. The sandstones are occasionally slightly oxidized. In the Mołdawa borehole, grey–cherry sandstones also occur in the uppermost cycle. The cycles are characterized by the following lithofacies succession: GB $\rightarrow$ $S_{Fe\ (m,\ xi)}$ $\rightarrow$ $H_{f>s2}$ $\rightarrow$ $H_{f>s1}$ or $S_{Fe\ (m,\ xi)}$ $\rightarrow$ S_b $\rightarrow$ $H_{f>s2}$ $\rightarrow$ $H_{f>s1}$ (Figure 2E(a)). Fining-upward cycles without green sandstones were also observed, comprising the following associations: GB $\rightarrow$ S_m $\rightarrow$ S_{xi} $\rightarrow$ S_m $\rightarrow$ $H_{f>s2}$ $\rightarrow$ $H_{f>s1}$; GB $\rightarrow$ S_{xi} $\rightarrow$ S_m $\rightarrow$ M_m; S_{xi} $\rightarrow$ S_m $\rightarrow$ $H_{f>s2}$ $\rightarrow$ $H_{f>s1}$; S_{xi} $\rightarrow$ S_{lam} $\rightarrow$ S_w; S_{xi} $\rightarrow$ S_{lam} $\rightarrow$ $H_{f>s2}$ $\rightarrow$ $H_{f>s1}$; S_{xi} $\rightarrow$ S_m $\rightarrow$ $H_{f>s2}$ $\rightarrow$ $H_{f>s1}$; S_m $\rightarrow$ S_{lam} $\rightarrow$ M_m (Figure 2E(b)).

An additional element that occurs in the Mołdawa, Władysław, and Omięcin XI/3 boreholes in the upper part of the Middle Bathonian, above the fining-upward cycles, is a several-meter-thick interbed of organodetrital and/or sandy limestones, rusty in color, containing limonite and ferruginous ooids (lithofacies L). The Jurassic section in the Omięcin XI/3 borehole ends with the aforementioned carbonate complex; younger sediments were removed in this area during inversion of the Mid-Polish Trough.

4.1.6. Upper Bathonian and Callovian

The Upper Bathonian and Callovian section is lithologically highly diverse in the study boreholes. In the Wąglany, Gutwin, and Wyszmontów 1 boreholes, three complexes can be distinguished: coarsening-upward siliciclastic complex, carbonate complex, and sandstone complex. In the Mołdawa borehole, a non-gradational sandstone complex is observed instead of the middle carbonate complex, while the Władysław borehole section is composed almost exclusively of carbonates. In all of the above-mentioned boreholes, the uppermost Middle Jurassic deposits roofs are represented by a complex of limestones of varying thickness, usually several meters.

In the Wąglany borehole, the section begins with a complex represented by clastic deposits forming a coarsening-upward cycle. They constitute the association of TS_m $\rightarrow$ S_{lam} $\rightarrow$ S_w $\rightarrow$ S_{wbiot} $\rightarrow$ S_w $\rightarrow$ D $\rightarrow$ S_w $\rightarrow$ S_{xi} $\rightarrow$ $S_{r,f}$ (Figure 2F). The sandstones are fine-grained, mostly dolomitized, grey and light grey in color, and contain infrequent bivalves and a single *Ophiomorpha* isp. in lithofacies S_{xi}.

A similar section was also found in the Gutwin borehole, although it started with a conglomerate level (lithofacies GB), and the overlying deposits represented the association of TS_m $\rightarrow$ S_w $\rightarrow$ S_{wbiot} $\rightarrow$ S_f + S_w $\rightarrow$ S_m $\rightarrow$ Sl_{am} + S_m. The sandstones are mostly fine-grained but medium-grained in the upper part, cemented with silica–clay cement, and light grey and light creamy in color.

In the Wyszmontów borehole, the small thickness and poor core recovery allow only the separation of lithofacies $H_{f>s2}$ $\rightarrow$ $H_{f>s1}$ $\rightarrow$ M_m in the lower part of the complex and upstream S_m and S_w. In the roofing part, there is a layer of medium-grained, massive chlorite sandstone (S_{Fe} lithofacies).

In the Mołdawa borehole, the lower complex is composed of three cycles, each starting with a conglomerate level (lithofacies GB). The conglomerates are overlain by: (1) massive

dark grey claystones (lithofacies M_m) containing small pebbles enveloped by limonite rims and yielding bivalve fossils; (2) a fining-upward cycle followed by massive coarse- to fine-grained sandstones (lithofacies S_m, upper in section association of lithofacies $S_m \rightarrow S_{lam} \rightarrow S_{xi}$), which are sideritized; brown-grey or light-grey in color; and contain siderite intercalations, limonite-coated sandstone pebbles, and sideritized clay clasts; and (3) grey–green fine-grained chlorite sandstones (lithofacies $S_{Fe,\,lam}$) that continuously pass into fine-grained, locally medium-grained sideritized sandstones representing lithofacies S_{lam}, grey–brown in color, containing plant roots and bivalve fossil levels.

The carbonate complex of the Upper Bathonian and Callovian is composed of limestones (lithofacies L) or dolomites (lithofacies D) several meters thick. In the Wąglany borehole, these are grey–cherry limestones showing tabular cross-bedding. In the Gutwin borehole, the section is represented by organodetrital limestones, rusty in color, abounding in dispersed limonite and iron ooids. The Wyszmontów 1 section is composed of sandy dolomites, rusty in color, with limonite and nest-like intercalations of limonite sandstones. In the Mołdawa borehole, the most likely equivalent of the carbonate complex is the complex of fine- and medium-grained dolomitized sandstones (lithofacies S_{lam}), light grey, containing clay clasts.

The upper sandstone complex in the study boreholes is also diverse in terms of lithofacies associations. In the Wąglany borehole, the association of lithofacies $S_{xt} \rightarrow S_{xi}$ and GB $\rightarrow S_{xt} \rightarrow S_{xi} \rightarrow S_{w,\,biot}$ form coarsening-upward cycles—from fine to medium grains. The sandstones are rust-colored, grey–green, or light grey-colored. They contain limonite or chlorite dispersed in the cement, ferruginous ooids, and clay clasts; in lithofacies $S_{w,biot}$, the trace fossil *Asterosoma* isp. was identified.

In the Gutwin borehole, the lithofacies association in this complex is GB $\rightarrow$ D $\rightarrow S_r \rightarrow S_{xi} \rightarrow S_w \rightarrow S_{Fe}$. The sandstones are fine-grained, mainly light grey, with ferruginous ooids and kaolinite in pores in the lower part. Grey–green chlorite sandstones occur in the uppermost part.

In the Mołdawa borehole, three fining-upward cycles are observed in the upper terrigenous complex (Figure 2G). The lower members of the cycles are represented by coarse- and medium-grained sandstones, while the upper members are composed of fine-grained sandstones. The lithofacies associations are $S_r \rightarrow S_m \rightarrow S_{xi} \rightarrow S_r$; $S_{xt} \rightarrow S_m$; $S_{xi} \rightarrow S_m$. The sandstones of the first cycle and the lower part of the second cycle are brown–grey in color, passing upward into a rusty grey. The entire section is rich in clay clasts. In its upper part, limonite and dolomitization also occur.

In the Wyszmontów 1 borehole, the upper terrigenous complex consists of fine-grained, massive (lithofacies S_m), calcareous, rusty-colored sandstones containing limonite in the cement and cherts.

A different Upper Bathonian and Callovian lithological section was found in the Władysław borehole. The entire 65.5-m-thick section is composed of organodetrital limestones, rusty in color, with crinoids and abundant limonite. They are also sideritized in the lower part.

Similar organodetrital (crinoid) limestones or sandy limestones with limonite, rusty in color, were found at the top of the Callovian in all the study boreholes. Their thicknesses range from several tens of centimeters (Wyszmonów 1) to several meters (Mołdawa).

4.2. Petrology

Siderite rocks are most often represented by clayey siderites and sideritic sandstones, subordinate coquinas, claystones, mudstones, and sideritic conglomerates [28,30].

4.2.1. Clayey Siderites

This group of rocks also includes muddy and sandy varieties (Figure 3A–H). Usually, these are dark brown rocks, compact, and occur in the form of beds or lenses and concretions.

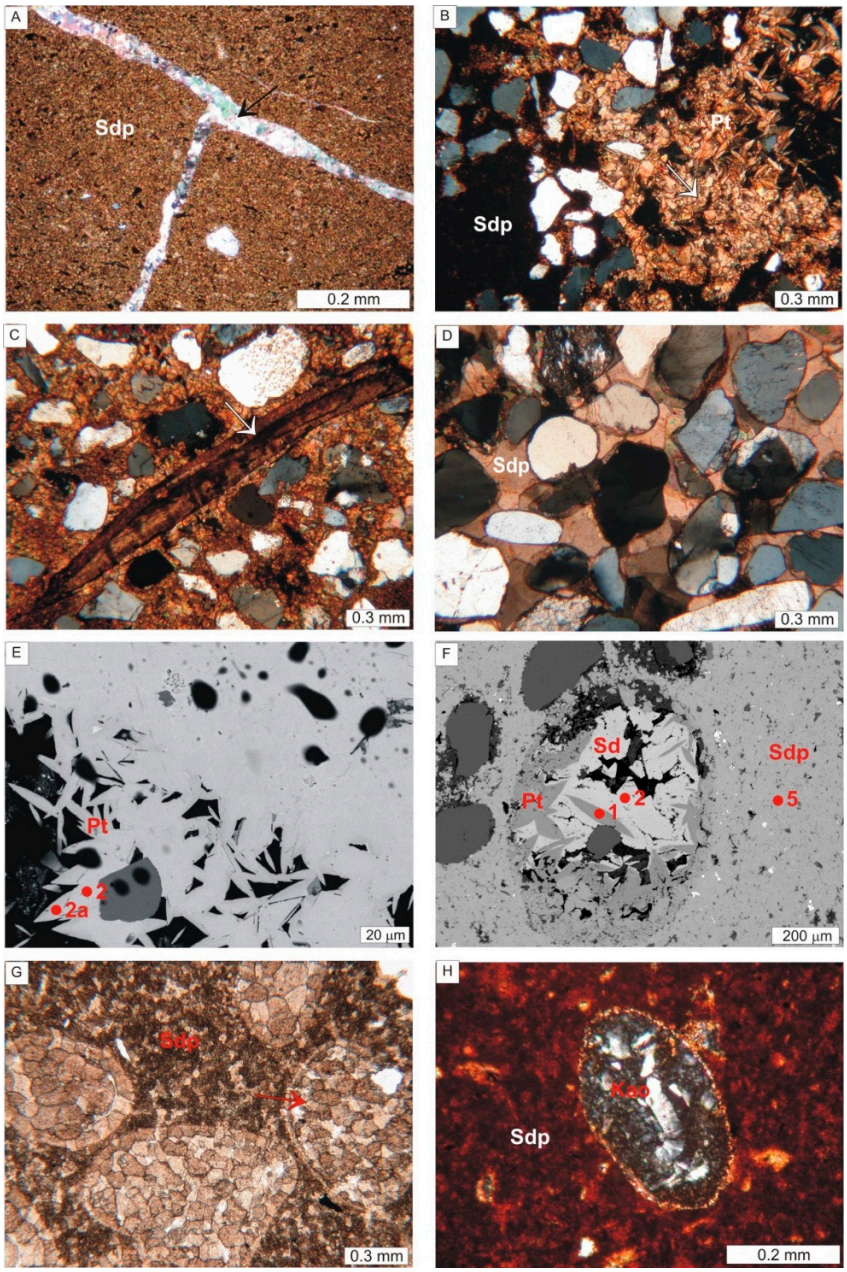

Figure 3. Photomicrographs of siderite rocks in polarizing microscope (PL) and scanning electron microscope (BSE). (**A**) Clayey siderite built of a sideroplesite micrite (Sdp) cut by a calcite vein (arrow); Mołdawa borehole, depth 304.5 m, PL—crossed nicols. (**B**) Sideroplesite micrite (Sdp), microsparite sideroplesite (arrow), and sparite rhomboedrons of pistomesite (Pt) in clayey-sandy siderite; Omięcin XI/3, depth 132.2 m, PL—crossed nicols. (**C**) Clayey-sandy microsparite siderite with fragment of a brachiopod shell (arrow); Gutwin borehole, depth 176.3 m, PL—crossed nicols. (**D**) Clayey-sandy siderite with spary sideroplesite cement (Sdp); Omięcin XI/3 borehole, depth 225.0 m, PL—crossed nicols. (**E**) Rhomboedrons of pistomesite (Pt) with a weakly visible zonal structure in a cement of clayey-sandy siderite; points of chemical analyses (EDS) in siderite (Table S2); Omięcin XI/3 borehole, depth 132.2 m, BSE image. (**F**) Siderite (Sd)–pistomesite (Pt) ooid in clayey-sandy siderite built of a sideroplesite micrite (Sdp); points of a chemical analyses (EDS) in siderite (Table S2); Wąglany k/Opoczna borehole, depth 597.2 m, BSE image. (**G**) Sideroplesite ooids (arrow) in clayey-sandy siderite built of a sideroplesite microsparite (Sdp); Wąglany k/Opoczna borehole, depth 395.2 m, PL—one nicol. (**H**) Kaolinite ooid (Kao) in clayey siderite built of a sideroplesite micrite (Sdp); Justynów PIG 1 borehole, depth 20.3 m, PL—crossed nicols.

The main components of clayey siderites are minerals of the siderite–magnesite isomorphic series (50–98 vol.% of rock) (Table S1). The energy-dispersed electron microscope study shows that it is mainly sideroplesite that contains 72.1–87.3 mol% $FeCO_3$, 3.0–20.3 mol% $MgCO_3$, 2.6–16.1 mol% $CaCO_3$, and 0.0–6.0 mol% MnCO3 (Table S2 and Figure 4). The two analyzed specimens represent siderite and seven represent pistomesite [86]. Sideroplesite and siderite occur as anhedral crystals, micrite (1–4 μm, [87]; Figure 3A,B) or microspar (4–20 μm; Figure 3B,C) in size. In addition, there are also spar specimens (>20 μm) that often show a rhombohedral habit (Figure 3B,D,E). Rhombohedral-shaped crystals are usually characterized by a higher $MgCO_3$ content (up to a maximum of 32.1 mol%, Table S2). Their chemical composition corresponds to sideroplesites and pistomesites. The BSE images of the sideroplesite and pistomesite cements show different chemical compositions, which are demonstrated by different shades of grey (Figure 3E,F). A darker color indicates a higher magnesium content. The analysis shows that the amount of magnesium in its chemical composition increased during the crystallization of sideroplesite. In places, sideroplesite spherulites were observed. Sideroplesite crystals are colorless or beige, and their edges are tinted with brown, while micrite-sized, finely crystalline aggregates are always dark brown.

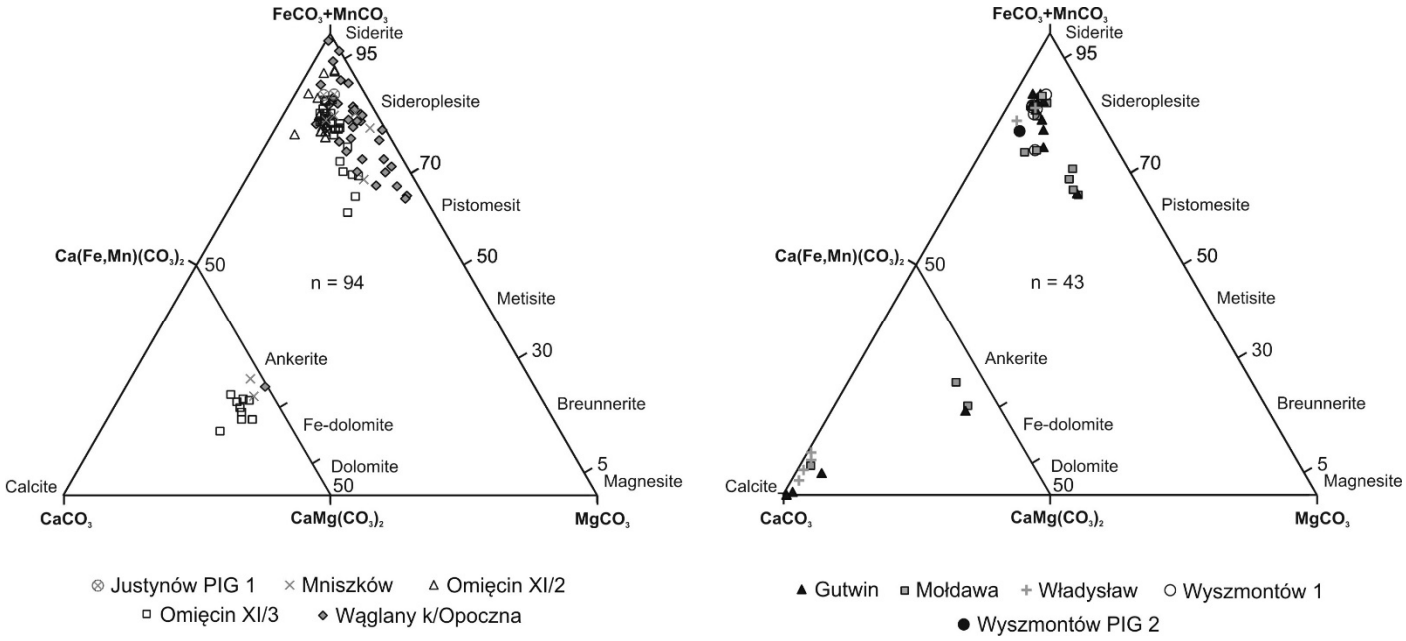

Figure 4. Ternary plot of the carbonates composition in mol %; *n*—analysis number.

The clayey siderites contain not only sideroplesite but also clay pelite (0–35 vol.% of rock), impregnated in places with organic matter or iron hydroxides. Clay minerals that occur in siderites are represented by very fine, colorless, low-birefringent flakes, probably representing mainly kaolinite. The green and yellow clay minerals represent berthierine and illite, as evidenced by X-ray studies [28]. Ankerite and less frequent calcite occur in varying amounts in the clayey siderites. The mineral composition of carbonate cements from the tested samples is presented in Table S2 and in the classification triangle (Figure 4). Quartz grains of the aleurite and psammite fractions account for 1.0–49.0 vol.% of rock, while feldspar grains (microclines), mica flakes (muscovite), coalified plant remains, and pyrite concentrations usually do not exceed 1.0 vol.%. Accessory constituents are also represented by zircon. The highest content of plant debris was recorded in the Wyszmontów PIG 2 borehole (depth 30.7 m-6.3 vol.%). A large amount of pyrite (12.7 vol.% was found at a depth of 125.0 m in the Wyszmontów 1 borehole.

The amounts of bioclasts and ooids in the clayey siderites do not exceed 18.0 vol.% of rock. In contrast, siderite intraclasts are usually represented by trace amounts. Bioclasts

occur mainly as fragments of shells: bivalves, brachiopods and gastropods, echinoderm plates, foraminifera tests, and serpulid tubes (Figure 3C). They are commonly composed of calcite and less frequently of sideroplesite and pyrite. Locally, they may constitute about 10.0 vol.% of rock (Wyszmontów 1, depth 84.6 m, and Omięcin XI/3, depth 184.4 m). Ooids in the clayey siderites have been observed rarely. The ooids are composed of berthierine that has been commonly replaced by sideroplesite, pistomesite, calcite, ankerite, or kaolinite (Figure 3F–H), [28]. Locally, the clayey siderites are intersected by veinlets filled with pyrite or calcite (Figure 3A).

4.2.2. Sideritic Sandstones

These are compact grey–brown rocks representing mainly fine- and medium-grained quartz arenites, locally very fine- and coarse-grained (Figure 5A–G). The detrital material is dominated by angular quartz grains (29.2–76.3 vol.% of rock) (Table S3). Potassium feldspar grains and muscovite and biotite flakes are minor constituents that most often account for approximately 1.0 vol.%. The highest feldspar content (5.7 vol.% of rock) was recorded in the Gutwin borehole (depth 207.95 m), while the mica content in the Omięcin XI/3 borehole was 11.7 vol.%; depth 210.2 m. In addition, single grains of heavy minerals (mainly zircon), pyrite aggregates, scattered plant detritus, kaolinite, and hematite were observed in the sandstones. Pyrite is most often present in trace amounts, except for samples from the Omięcin XI/2 borehole, where the maximum pyrite content is over 30.0 vol.% of rock. The content of plant detritus in most of the analyzed samples does not exceed 1.0 vol.% of rock, and the highest percentage is 5.0 vol.% (Omięcin XI/3, depth 210.2 m).

Bioclasts, ooids, and siderite concretions occur in varying amounts. The most common bioclasts include bivalves, echinoderms, gastropods, and foraminifers (Figure 5A). The fossil fragments are composed commonly of calcite and, in places, of ankerite, siderite, kaolinite, pyrite, and phosphates. In the cathodoluminescent image, the calcite bioclasts are characterized by red–orange color, while the phosphate is yellowish-grey. An analysis of the calcite shells in an electron microprobe shows that it is manganese-free calcite (Table S2). The contents of the fossil clasts are most often around 1.0 vol.%; however, in some places, they exceed 10.0 vol.%.

Ooids in the sideritic sandstones are quite common. Their contents range from 0 to 55.7 vol.% of rock. Ooids form oval grains, less often spherical, with diameters of 0.1–1.0 mm. Their cores usually contain quartz grains or small bioclasts. Ooids are composed of a green or yellow–brown mineral—berthierine (Figure 5B). This mineral was identified by X-ray examinations. The chemical composition of berthierine in ooids was determined in two samples [28] yielding the following results: 25.59–29.29 wt% FeO, 31.42–35.41% SiO_2, 20.08–28.40% $Al2O_3$, 0.00–5.44% MgO, 0.08–1.13% CaO, and 0.00–0.44% MnO. The cortex of berthierine ooids showed a poorly outlined concentric structure. The ooids were often carbonated; berthierine was replaced by calcite, ankerite, sideroplesite, or pistomesite and pyrite (Figure 5C). The amount of intraclasts in some of the tested samples was mainly in the range of 1.0–3.0 vol.%, with a maximum of 5.0 vol.% (Omięcin XI/3, depth 172.9 m).

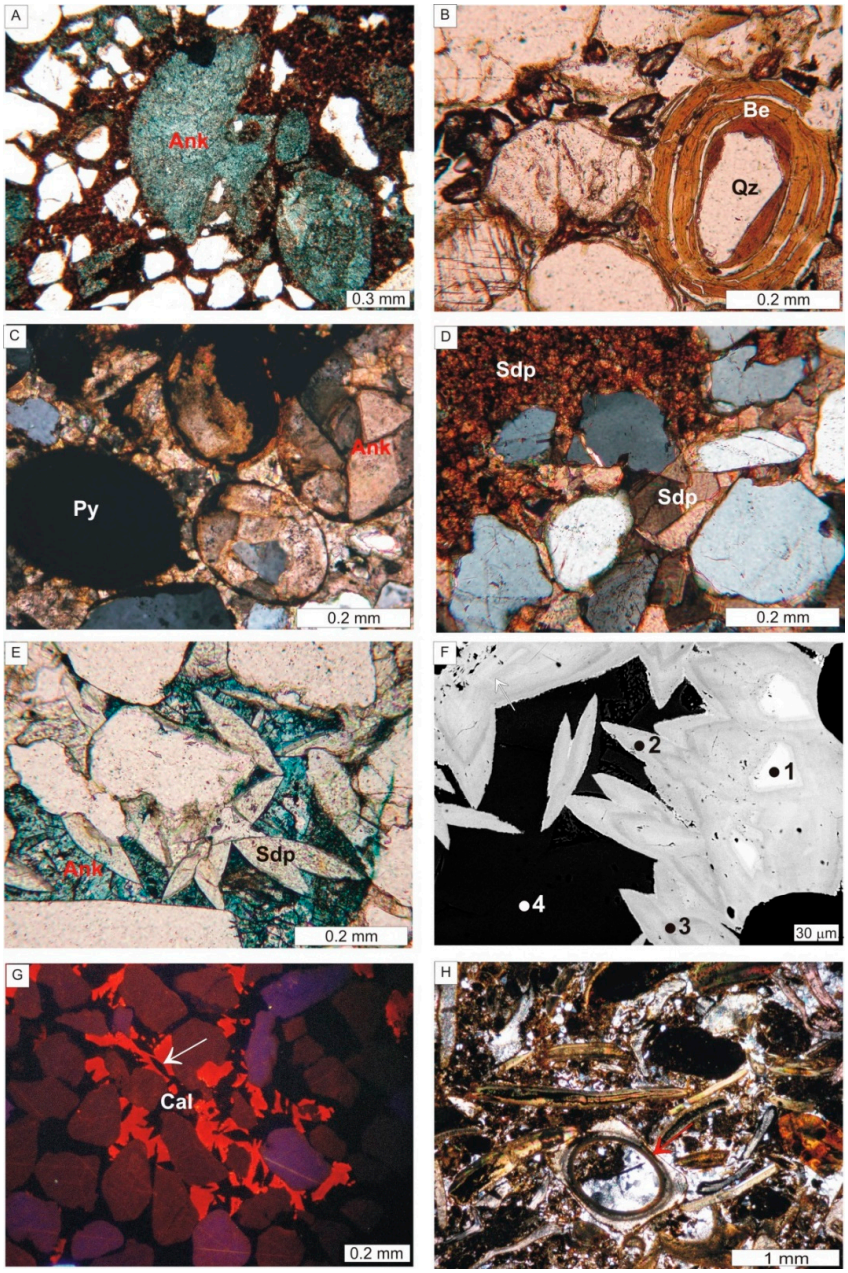

Figure 5. Photomicrographs of siderite rocks in polarizing microscope (PL), cathodoluminescence (CL), and scanning electron microscope (BSE). (**A**) Sideritic sandstone with micrite sideroplesite cement (Sdp). Note ankeritic bioclasts (Ank—blue color); Mniszków IG 1borehole, depth 916.9 m, PL—one nicol. (**B**) Berthierine ooid (Be) with concentric lamellae and quartz (Qz) nucleus in sideritic sandstone; Gutwin borehole, depth 124.2 m, PL—one nicol. (**C**) Ankerite (Ank) and pyrite (Py) ooids in sideritic sandstone; Wąglany k/Opoczna borehole, depth 482.7 m, PL—crossed nicols. (**D**) Microsparite and sparite sideroplesite (Sdp) in sideritic sandstone; Gutwin borehole, depth 207.95 m, PL—crossed nicols. (**E**) Rhomboedrons of sideroplesite (Sdp) and ankerite (Ank) cement in sideritic sandstone; Mołdawa borehole, depth 243.5 m, PL—one nicol. (**F**) Rhomboedrons of sideroplesite–pistomesite with a zonal structure in sideritic sandstone; points of chemical analyses (EDS) in siderite (Table S2); Mołdawa borehole, depth 243.5 m, BSE image. (**G**) Fragment of sideritic sandstone, CL image. Nonluminescent rhomboedrons of sideroplesite (arrow) and red luminescence of calcite (Cal) cement; Gutwin borehole, depth 201.6 m. (**H**) Fragments of serpulid tube (arrow) and bivalve shells in sideritic conquina; Wyszmontów 1 borehole, depth 99.3 m, PL—crossed nicols.

The sandstones are cemented predominantly with carbonate minerals and, to a lesser extent, clay minerals. Among the carbonate minerals, micritic and microsparitic sideroplesite, sparitic sideroplesite and pistomesite, ankerite, and Fe-calcite were found (Figure 5A–G). Sideroplesite spherulites were observed in some places. The contents of sideroplesite and pistomesite ranged from 0.7 to 49.0 vol.% of rock. The sideroplesites analyzed in the EDS electron microscope were characterized by the following chemical composition: 75.4–87.2 mol% $FeCO_3$, 3.9–22.5 mol% $MgCO_3$, 0.4–17.3 mol% $CaCO_3$, and 0.0–4.2 mol% $MnCO_3$ (Table S2 and Figure 4). The determinations made on pistomesite crystals showed the following contents: 64.3–69.9 mol% $FeCO_3$, 18.0–26.3 mol% $MgCO_3$, 2.9–12.3 mol% $CaCO_3$, and 0.6–3.2 mol% $MnCO_3$ (Table S2 and Figure 4). The backscattered electron (BSE) image of sideroplesite and pistomesite crystals may reveal differences in the chemical composition of the minerals. Some of the microsparite crystals of sideroplesite are characterized by a slight difference in the chemical composition between its outer and middle parts. Within the sideroplesite and pistomesite rhombohedrons, a zonal structure is often observed, marked by oscillations in the iron and magnesium proportions (Figure 5E,F). The sideroplesite and pistomesite cements of the sandstones are frequently accompanied by ankerite (Figure 5F). Both calcite and ankerite were found in samples from the Gutwin, Mołdawa, Omięcin XI/2, and Władysław boreholes. Exclusively, calcite was recorded in sideritic sandstones of the Wyszmontów 1 borehole, and ankerite was the only one found in the Mniszków IG 1, Omięcin XI/3, and Wąglany boreholes. In the cathodoluminescence analysis, the calcite cements were red–orange in color (Figure 5G). The sideritic sandstones were cut in places by veinlets filled with calcite or ankerite and sideroplesite or pistomesite. There was also a sideroplesite vein whose outer parts of sideroplesite crystals were characterized by a higher magnesium content than the inner parts.

4.2.3. Sideritic Conquinas

Jurassic sideritic coquinas described in the literature are rocks in which bioclasts definitely prevail over carbonate components of the cement [6,21–23]. In the present paper, this name refers to clayey siderites containing more than 20 vol.% of bioclasts in the rock (Figure 5H and Table S4). There are only three samples that represent this rock group. Among the detrital grains, the most common is quartz of silt or sand size, while the amount of feldspars is small. Accessory components are represented by pyrite and plant detritus. The proportion of clay or ferruginous-clay pelite is variable. The X-ray analysis showed the presence of berthierine. All samples contain ooids composed of berthierine that has been partially or completely replaced in some places by calcite, ankerite, sideroplesite, or pyrite. Intraclasts occur locally. Bioclasts are represented by fragments of echinoderms, bivalves, brachiopods, gastropods, bryozoans, and serpulid tubes (Figure 5H). The cathodoluminescence research showed that calcite bioclasts are orange–red in color. In places, the bioclasts are replaced with brownish phosphate. The grain material is cemented mostly with sideroplesite, ankerite, or calcite.

4.2.4. Sideritic Claystones and Sideritic Mudstones

These are brown rocks showing a pelitic–aleuritic structure and a directional texture, emphasized by the arrangement of micas, siderite, and organic matter. Carbonate minerals are represented only by micritic sideroplesite that vary in percentage from 20 vol.% to 30 vol.% of rock. The detrital material includes quartz silt and sand (10–30 vol.% of rock) and micas (7–20 vol.% of rock), predominantly muscovite. Plant detritus is common, on average around 3 vol.% of rock.

4.2.5. Sideritic Conglomerates

Five samples were included in this group of rocks and defined as poly- and oligomictic paraconglomerates due to the nature of psephitic clasts [28].

Polymictic paraconglomerates are found in the Justynów IG 1 (depth 26.0 m) and Mołdawa (depths 153.1, 303.9, and 326.6 m) boreholes. The psephitic grains are represented

by clasts of the following rocks: clayey siderite, sideritic claystone, sandstones cemented with ankerite, calcite or berthierine, carbonates, and mono- and polycrystalline quartz. The groundmass that fills the conglomerates is a sandy matrix, locally with bioclasts and ooids, and cements: sideroplesite (micrite and microspar), calcite, and berthierine.

Oligomictic paraconglomerate occurs in the Omięcin XI/3 borehole (depth 109.1 m). Clasts of calcitic–sideritic sandstone are cemented with micritic sideroplesite.

4.3. Isotopic Studies

The determination of an isotopic composition of carbon and oxygen was performed mainly on clayey siderites and sideritic sandstones, in which iron carbonate is represented exclusively or mostly by finely crystalline sideroplesite and siderite (Table S5). Moreover, studies of two samples containing rhombohedral crystals of pistomesite and sideroplesite were made. Additionally, carbon and oxygen isotopes were determined in the calcite cement.

The $\delta^{13}C_{VPDB}$ values of sideroplesites and siderites range from –24.58‰ to +1.51‰$_{VPDB}$ (VPDB is Vienna Peedee Belemnite). The values of $\delta^{18}O$ ‰$_{VPDB}$ of finely crystalline sideroplesites and siderites vary between −8.87‰ and +3.97‰$_{VPDB}$, which gives values from 21.71 to 31.50‰$_{VSMOW}$ (VSMOW is Vienna Standard Mean Ocean Water). The two determinations in rhombohedral crystals of sideroplesite and pistomesite are −8.82 and −10.45‰$_{VPDB}$, respectively (21.77 and 20.08‰$_{VSMOW}$). Figure 6 illustrates a graph of the isotopic compositions of oxygen and carbon in sideroplesites and pistomesite. We can see that the $\delta^{13}C_{VPDB}$ values of most of the analyzed sideroplesites range from about −15.00 to 0.00‰$_{VPDB}$, while the $\delta^{18}O$‰$_{VPDB}$ values are from about −6.00 to +2.00‰$_{VPDB}$.

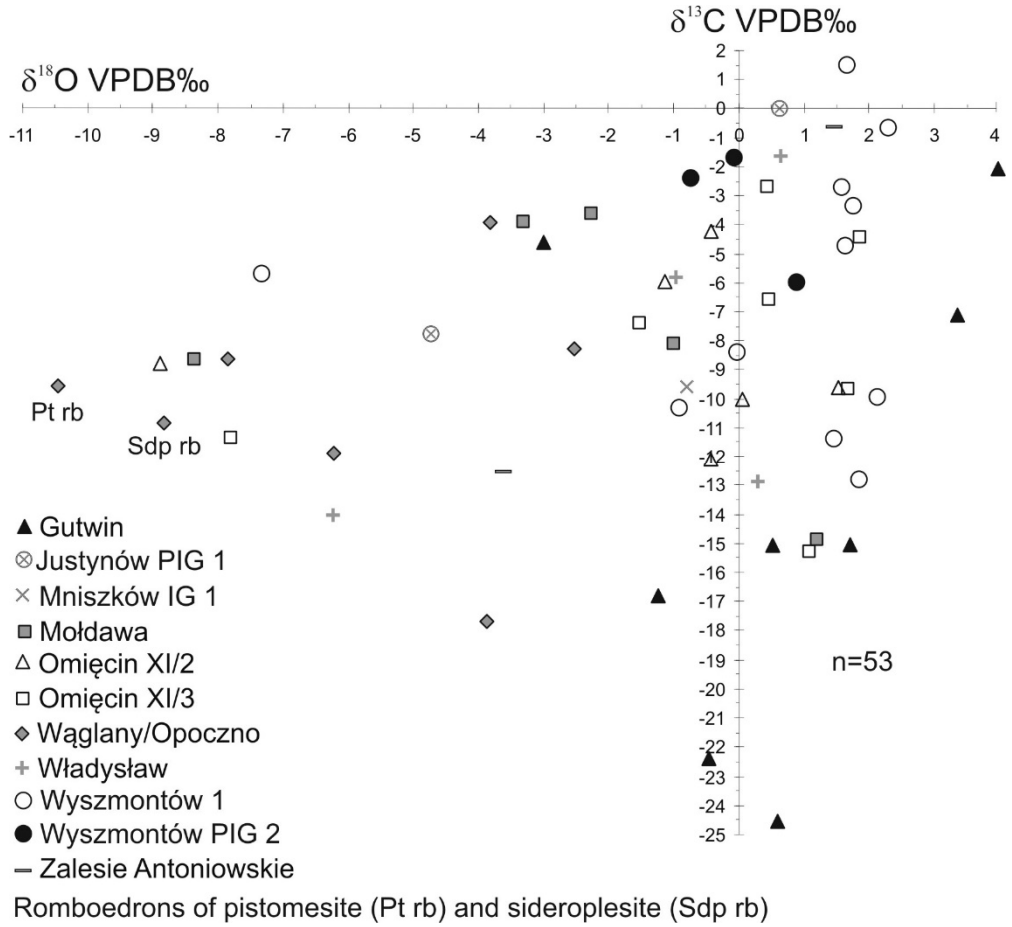

Figure 6. Plot of $\delta^{18}O_{VPDB}$‰ versus $\delta^{13}C_{VPDB}$‰ in siderite cements.

Determination of the oxygen and carbon isotopes was also performed in the calcite cement of sideritic sandstone of the Wyszmontów 1 borehole. The $\delta^{13}C$ value is $-11.15‰_{VPDB}$, and the $\delta^{18}O$ value is $-4.45‰_{VPDB}$ ($26.27‰_{VSMOW}$, Table S5).

The isotopic composition of oxygen and carbon in ankerite was examined in two samples of quartz sandstones cemented with the carbonate in the Wąglany borehole. The $\delta^{13}C$ values are -7.04 and $-6.54‰_{VPDB}$, and the $\delta^{18}O$ values are -10.63 and $-10.63‰_{VPDB}$ (19.91 and $20.54‰_{VSMOW}$) [30].

5. Interpretation and Discussion

5.1. Sedimentary Environments

Interpretation of the sedimentary environments was made based on the vertical sequence of lithofacies in individual wells in conjunction with the interpretation of their mechanism of deposition. Then, a correlation of environments between the boreholes was made (Figure 7).

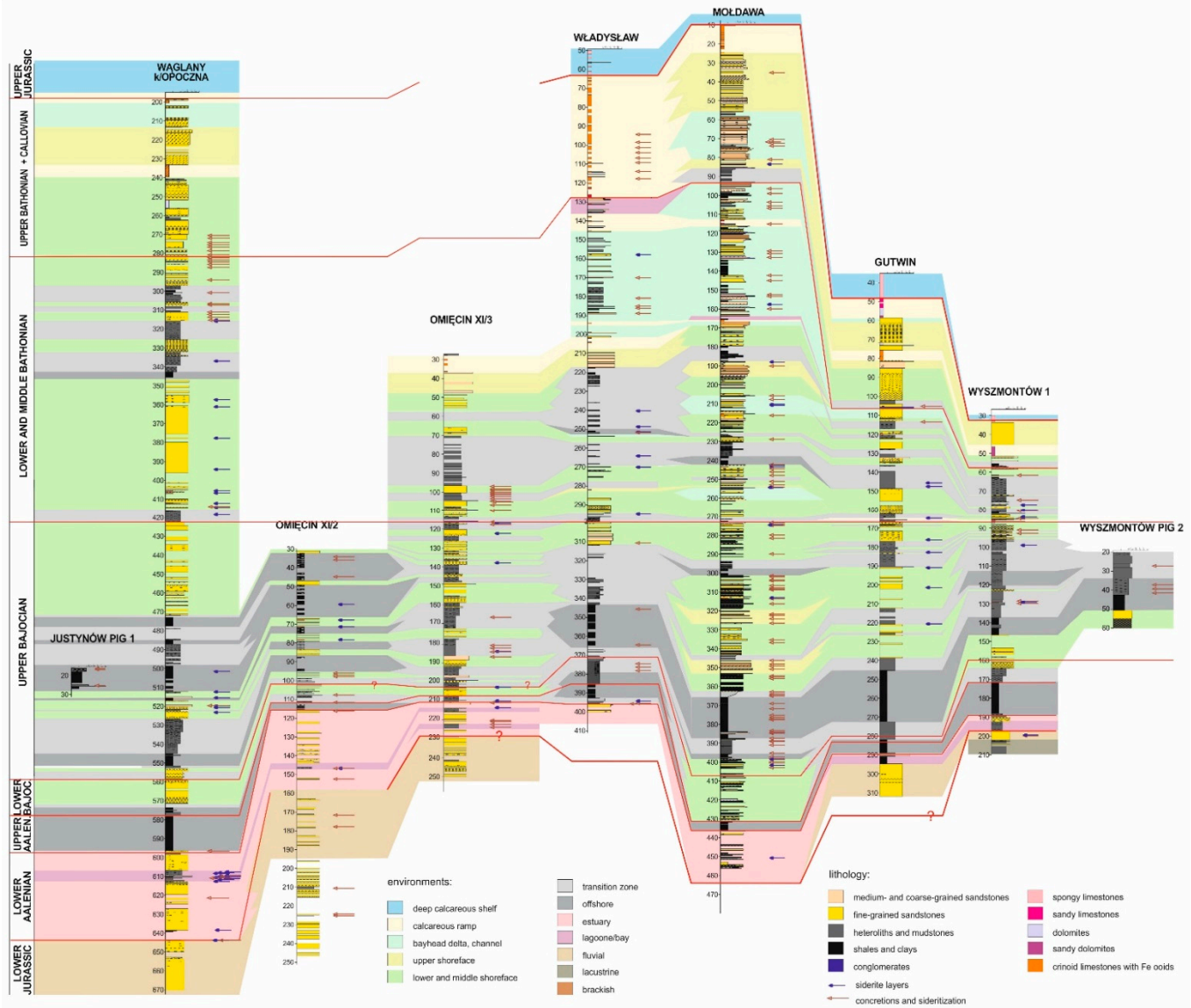

Figure 7. Correlation of the Middle Jurassic sediments between studied boreholes.

5.1.1. Lower Aalenian

Sedimentation of the Lower Aalenian deposits took place in a marine or brackish environment. This is evidenced by the presence of bivalve fossils and infrequent foraminifera specimens found in the fine-grained types of facies.

The section is dominated by lithofacies S_m and S_{lam}, the formation of which is associated with relatively strong density currents, fast sediment deposition, and the lack of further reworking of the sediment by waving. Massive sandstones (S_m) are known from a few environments, including estuary channels [88–90]. Clay streaks (a characteristic element of lithofacies S_{lam}), many of them rich in carbonaceous detritus and muscovite, are associated with rare calm periods of deposition from suspension. Their presence is reported as a characteristic feature of deposits that accumulate in the subtidal zone [91,92].

The less frequently observed sandstones of lithofacies S_f and S_w are an indicator of the alternating deposition of sand by traction currents and clay from suspension in the absence of flow. Such conditions are common in tidal zones. Flasher and lenticular bedding observed in this lithofacies is characteristic of both a sand flat in the intertidal zone and the marginal parts of channels in the subtidal zone [60]. It has also been found in the deposits of incised valleys that formed at the initial stage of transgression [90,93].

The presence of *Skolithos*, *Palaeophycus*, and *Dipplocraterion* trace fossils is diagnostic for the shallow-marine Skolithos ichnofacies [94]. Particularly important for the interpretation of the environment is the presence of *Dipplocraterion* isp., which is often found in the environments of tidal sand flats and estuary channel sediments [65].

Based on these features, the sedimentary environment of the Lower Aalenian deposits in the N and NE margins of the Holy Cross Mountains was interpreted as a tidal-dominated estuary [95]. The sandstones of high-energy lithofacies were deposited within channel facies, the remaining ones within a tidal sand flat [96]. Sedimentation of the mudstone heteroliths should be related to a mud flat characteristic of the middle section of tide-dominated estuary. The presence of low-angle cross-bedding found in the Wyszmontów 1 borehole suggests that these deposits were accumulated within a shallower coastal area or an outer zone of estuary, where slight effects of waves and storms were already marked. The massive claystones containing bivalves, foraminifera, and siderite interbeds found in the middle and lower part of the section were deposited in lagoons or marginal parts of the estuarium, probably near saline marshes, i.e., in places of a significant supply of iron ions to the sediment.

The interpretations presented herein are consistent with that demonstrated for the Lower Aalenian deposits thoroughly analyzed in the central part of the Mid-Polish Trough [67,74,97] also interpreted as estuarine deposits, as well as with the regional palaeogeographic patterns and the supposed direction of marine transgression at the beginning of the Middle Jurassic [79,98].

5.1.2. Upper Aalenian and Lower Bajocian

The Upper Aalenian section should be interpreted combined with the Lower Bajocian section. It is a coarsening-upward section, in which the lithofacies succession is characteristic of a progradation of the coast of a vast shallow epeirogenic sea [62,66] (Figure 2B). The lower part of the section, which comprises fine-grained massive lithofacies (M_m and T_m) or those containing a few millimeter-thick silt laminae (M_{lam} lithofacies) and marine fossils were deposited from suspension in a very calm marine environment below the storm wave base. The black color of the deposits suggests oxygen deficiency conditions. The isolated silt laminae, increasingly frequent upward in the section, which continue for a few centimeters (lithofacies $H_{f>s1}$), were probably deposited as a result of activity of low-density currents of very low velocity [99]. These deposits are interpreted as accumulated in an offshore area.

The overlying lenticularly bedded heteroliths and equicomponent lenticularly and wavy-bedded heteroliths indicate a highly variable energy of the environment. Periods of clay deposition from suspension in the absence of water movement were frequently

interrupted by periods of current flows or storms. The lenses composed of fine-grained sandstones are the results of activity of either currents poor in sand materials, which formed isolated ripples, the so-called starved ripples, on a muddy substrate (lithofacies $H_{f>s2}$) [60,100,101] or currents rich in sand materials that formed thin layers (lithofacies $H_{f=s}$). The laminated lenses were also interpreted by Dott and Bourgeois [102] as equivalents to micro-hummocky bedding. They presumably represent relict storm ripple marks, in which the sand material transported by storms has been preserved.

The dominant ichnofossils in these rocks are *Chondrites* isp. and *Planolites* isp., representing the *Cruziana* ichnofacies that is characteristic of depths below the fairweather wave base [65]. The position in the section allows for the interpretation of these deposits as representing a transition zone between the shoreface and offshore [60], located between the storm and fairweather wave bases.

The wavy-bedded, very fine- and fine-grained sandstones (lithofacies S_w), massive (S_m), and with clay streaks (S_{lam}), which are dominant in the upper part of the section, indicate an increasing supply of sand material and a continuation of a shallowing trend. These deposits were accumulated near and then above the fairweather wave base in the lower shoreface environment.

The Upper Aalenian-Lower Bajocian section of the N and NE margin of the Holy Cross Mountains shows the same trend and succession of sedimentary environments as those observed in the central part of the Polish sedimentary basin [67,68,103].

5.1.3. Upper Bajocian

The Upper Bajocian coarsening-upward cycles are very similar to the above-described progradational cycle characterizing the Upper Aalenian and Lower Bajocian sections (Figure 2C). An additional feature is the presence of sandstone interbeds of lithofacies S_{xl} or S_m, bounded at the base by sharp boundaries, in heteroliths, and in wavy-bedded sandstones. These types of interbeds within the deposits of offshore and transitional zones represent a member of a storm-related tempestite sequences [62]. Their presence in these sections is considered indicative for depths below the fairweather wave base [104–108].

The trace fossils of *Chondrites targioni* Brongniart, *Planolites* isp., *Planolites beverleyensis* (Billings), *Schaubcylindrichnus* isp., and *Gyrochorte comosa* Heer, observed at the bottom of the cycles, are the common features of the *Cruziana* ichnofacies [65].

The upper members of the Upper Bajocian cycles are characterized by the presence of thick massive sandstones (S_m) and sandstones with clay laminae (S_{lam}). A lack of bedding in the sandstones may be caused by several original factors: fast deposition from rapidly slowing turbidity currents, mass deposition from highly concentrated gravity flows, and deposition from traction currents under the upper flow regime conditions (antidune phases) [109]. In the Upper Bajocian section, their formation is most likely related to the rapid deposition of sand carried by currents or storm waves directly from suspension. It is also possible that some of the original sedimentary structures have been blurred as a result of sediment liquefaction [101].

The medium- and coarse-grained sandstones that form the S_{xi} lithofacies, occurring in the uppermost parts of the cycles in the Mołdawa borehole, indicate a higher-energy environment in which moderately strong traction currents of the "phase of lower flow regime dunes" operate. It is usually the result of migration of large ripple marks [101].

The sedimentation cycles found in the Upper Bajocian section are typical progradational cycles from the offshore, through the transitional zone to the lower or middle shoreface, and in the Mołdawa borehole also the upper shoreface.

5.1.4. Lower and Middle Bathonian

Coarsening-upward cycles (Figure 2D) comprise much of the Lower and Middle Bathonian section, like in the Bajocian. Some of them, especially those found in the lower parts of the sections (excluding the Wąglany borehole), start with a conglomerate level. These levels are indicative of sedimentary or erosional gaps between the cycles. Lithologies

of the lower and middle parts of the cycles are the same as their counterparts from the Upper Bajocian and represent the offshore environment and the transitional zone between the offshore and shoreface. Fine-grained, highly bioturbated deposits are more common within them, which prove a lower rate of basin subsidence.

The upper parts of the cycles observed here show greater diversity. Most of the cycles, as in the Upper Bajocian, are dominated by lithofacies S_m and S_{lam}, which have been interpreted as indicative for the lower and middle shorefaces. In the Gutwin and Wyszmontów boreholes, sandstone packets with low-angle cross-bedding (lithofacies S_{xl}) (Figure 2D), which is interpreted as hummocky cross-stratification (HCS) [50] are an indicator of storm-dominated environment. They contain trace fossils of *Palaeophycus* isp representing a component of *Skolithos* ichnofacies. The above-mentioned features allow interpreting this part of the section as deposited in the lower or even middle shoreface zones [62,65,110–112]. In the upper cycle of the Wąglany borehole, we can also observe streaky bedding (lithofacies S_f), less often ripple bedding (lithofacies S_r) and trough cross-bedding (S_{xi} lithofacies), with scarce ichnofossils representing the *Skolithos* ichnofacies (*Skolithos* isp., *Palaeophycus* isp., and *Ophiomorpha* isp.). The former two lithofacies are associated with a shallow environment of the middle or upper shoreface (area of intertidal sand flat, shallows, and shoals) [60]. Lithofacies S_{xi} indicate the effect of moderately strong traction currents in the "phase of lower flow regime dunes" and form usually as a result of migration of large ripple marks [101] in the upper shoreface zone.

The fining-upward cycles (Figure 2E) observed in the upper part of the Middle Bathonian section in the Mołdawa and Władysław boreholes are associated with a different sedimentary environment. They start with either conglomerates or coarse- or medium-grained sandstones with a sharp lithological boundary, which indicates the erosional nature of the basal surfaces of the cycles. This type of cyclicity is usually related to fluvial deposition. However, the characteristic feature of the sandy members of many cycles in the sections under discussion is the presence of chlorite sandstones, massive or with thorough cross-bedding, and bivalve fossils. According to Worden et al. [113], large amounts of chlorite in sandstones form in zones where waters, rich in iron compounds carried by rivers, flow into the marine basin and encounter salty waters, i.e., in an environment of reduced salinity (delta estuary). Worden et al. [113] showed that the most favorable place for the formation of chlorite minerals is the proximal part of a tide-dominated estuary [95], the so-called bayhead delta. The fining-upward sections observed in the NE margin of the Holy Cross Mountains, which contain sedimentary structures indicating a high-energy environment and a significant amount of chlorite, should therefore be interpreted as formed in the estuary environment, in the zone of sand bars, and sand flats situated within the bayhead delta. The cycles end with fine-grained deposits that accumulate in a mud flat environment.

A several-meter-thick interbeds of organodetrital and/or sandy limestones, rusty color, with limonite and ferruginous ooids (lithofacies L), which occur at the top of the Middle Bathonian in the Mołdawa, Omięcin XI/3, and Władysław boreholes, presumably represent the outer or middle zones of the carbonate ramp (outer ramp and mid-ramp).

5.1.5. Upper Bathonian and Callovian

The Upper Bathonian and Callovian section in the study boreholes showed different facies types, which proves the presence of several sedimentary environments. The common features of the sections seem to be their tripartite nature and the presence of crinoid limestones with limonite, rusty in color, in the middle complex. These limestones are also observed in the entire section of the Władysław borehole and at the top of the Middle Jurassic in all the borehole sections.

The lower siliciclastic complex in the boreholes located in the northern margin of the Holy Cross Mountains (Wąglany, Omięcin XI/3) is characterized by a coarsening-upward section and the lithofacies succession that indicates an increase in the environmental energy (Figure 2F). Its formation is associated with a progradation from the transitional

zone, through the lower to the middle shoreface. In the Mołdawa and Gutwin boreholes, located further east of the sedimentary basin axis, the basal conglomerate level indicates an erosion event followed by a marine transgression and the sedimentation of fine-grained deposits (lithofacies M_m) with bivalve fossils, which probably took place in a lagoonal environment. In the Mołdawa borehole, the presence of overlying medium- and coarse-grained sandstones containing high-energy lithofacies (S_m and S_{xi}) with sandstone pebble levels and clay clasts, without fossils, indicates the environment of upper shoreface, sand bars, or river channel bars. The overlying lithofacies of chlorite sandstones (S_{Fe}) followed by sandstones (S_{lam}) containing levels of plant roots or bivalve fossils allow interpreting the entire sandstone complex with claystone intercalations at the top as representing a tidal-dominated estuary environment [95,113]. In the Gutwin borehole, this part of the section is dominated by index lithofacies for the intertidal sand flat (S_w and S_f) [60] and, then, for the higher-energy subtidal zone (lithofacies S_{lam}). The poor core yield and the small thickness of the section in the Wyszmontów 1 borehole allow only the interpretation that it is genetically similar to the section of the Mołdawa borehole in the lower part; fine-grained deposits with bivalve fossils suggest a lagoonal environment, while the presence of chlorite sandstones in the upper part point to an estuary environment.

The middle carbonate complex of all the sections, except in the Mołdawa and Wyszmontów 1, is composed of organodetrital limestones, usually rusty in color, in which crinoids are the most important rock-forming component. These limestones were deposited in a carbonate ramp/platform environment, mainly in a depth zone between the fairweather and storm wave bases (mid-ramp/platform, margin reef, and platform slope) [114]. The presence of tabular cross-bedding and the cherry color of these limestones in the Wąglany borehole suggest that the deposits are of allochthonous origin in this borehole. Their formation was likely associated with the transport of crinoids from shallower zones to the outer ramp zone, probably as a result of storms [114]. The equivalent of the crinoid limestones in the Mołdawa borehole are probably the dolomitized fine- and medium-grained sandstones of lithofacies S_{lam}, containing clay clasts and *Skolithos* isp., which should be most likely interpreted as upper shoreface deposits [65], accumulated on estuarine rocks during a progressive transgression. The greyish-rusty sandy dolomites with limonite and nest-like intercalations of limonite sandstones and belemnite fossils, found in the Wyszmontów 1 borehole, should be interpreted in a similar way.

The upper siliciclastic complex, present in the Wąglany, Mołdawa, Gutwin, and Wyszmontów 1 boreholes, is dominated by high-energy lithofacies (S_{xt}, S_{xi}, S_m, and S_r); however, in each of the boreholes, there are different relationships between them, indicating a slight differentiation of depositional environments.

In the Wąglany borehole, the lithofacies association of $S_{xt} \rightarrow S_{xi} \rightarrow S_{Fe,\,xi}$ with a coarsening-upward succession is interpreted as upper shoreface deposits. The overlying fining-upward sandstone cycle, in its upper part containing lithofacies S_w and S_{wbiot} with *Asterosoma* isp., indicates a progressive transgression and deepening of the marine basin. The indicator component, apart from the lithofacies succession, is the presence of *Asterosoma* isp., which is a component of the *Cruziana* ichnofacies and is commonly recorded in open-marine deposits in the upper part of the lower shoreface [65].

The four fining-upward cycles found in the Mołdawa borehole, from coarse-, through medium-, and to fine-grained sandstones (Figure 2G) are interpreted as deposited in the subtidal zone of tidal channels [62] located near a river that supplied large amounts of iron compounds from land.

The uppermost Callovian deposits in the Gutwin borehole accumulated in a slightly shallower environment. The sandstones, dominant above a conglomerate level, followed by a thin dolomite layer, are interpreted as deposited in the tidal sand flat [60].

In the Wyszmontów 1 borehole, the upper siliciclastic complex, containing fine-grained, massive (lithofacies S_m), calcareous, rust-colored sandstones with limonite in the cement and cherts is difficult to interpret. Based on the origin of rocks of the same age found in the remaining boreholes, their deposition was probably associated with

the shoreface zone located near the mouth of a river supplying large amounts of iron compounds from land.

5.2. Isotopes

The $\delta^{13}C$ values indicate that the sideroplesite and siderite were formed in the microbial methanogenesis zone where CO_2 originated from the bacterial fermentation of organic components [115]. Morad [116] reported that the values of $\delta^{13}C$ in carbonates that precipitate in this zone range from −22‰ to +2‰$_{VPDB}$. The values of the majority of analyzed samples fall within this range.

In order to calculate the $\delta^{18}O$ value of the crystallization water of sideroplesite, its temperature was assumed to 20 °C [117,118]. The relationship between the $\delta^{18}O$‰$_{VSMOW}$ of water and the crystallization temperature of sideroplesite is presented graphically in Figure 8 [119]. The $\delta^{18}O$‰$_{SMOW}$ values calculated for the water range from −12.17‰ to +1.07‰$_{VSMOW}$ (Table S5). The analyses of the oxygen isotopes from sideroplesites in the Wąglany, Justynów PIG 1, Mniszków IG 1, Omięcin XI/2, and Omięcin XI/3 boreholes indicate that the $\delta^{18}O$‰$_{VSMOW}$ values of pore water are lower and range from approximately −8.00 to −1.00‰$_{VSMOW}$ (Figure 8). These values indicate that the sideroplesite crystallized from water composed of meteoric water with an admixture of seawater. However, most of the samples from the Gutwin, Mołdawa, Władysław, Wyszmontów 1, PIG 2, and Zalesie Antoniowskie boreholes showed slightly higher $\delta^{18}O$‰$_{VSMOW}$ values of water, ranging from about −7.00 to + 1.00‰$_{VSMOW}$ (Figure 8). This may correspond to seawater or a mixture of seawater and meteoric water. To sum up, the pore waters, from which the diagenetic sideroplesite crystallized, were not homogeneous and originated from both marine and meteoric waters [29].

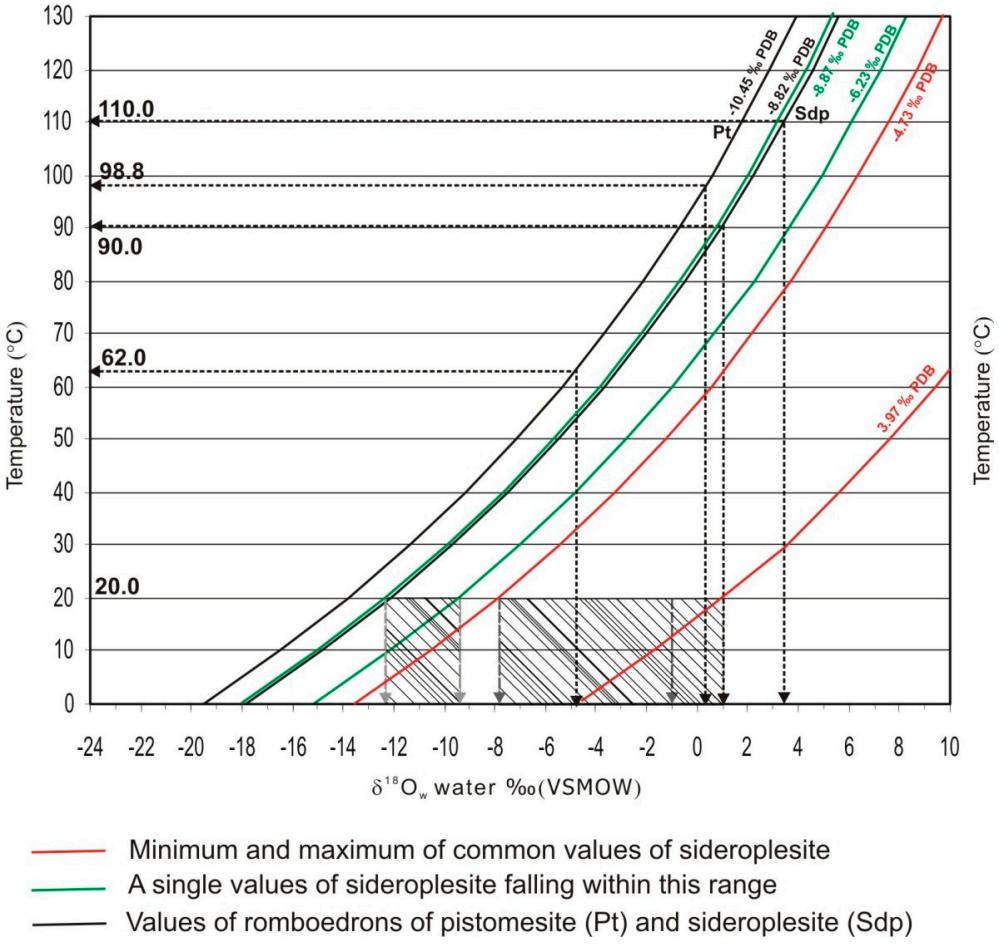

Figure 8. Plot of the $\delta^{18}O$ pore water versus temperature for siderite cements (after Reference [119]).

The average $\delta^{13}C$ and $\delta^{18}O$ values of sideroplesite in a given age range are as follows: −7.02 and −1.52‰ $_{VPDB}$ for the Aalenian, −5.80 and −0.77‰ $_{VPDB}$ for the Bajocian, and −12.26 and −0.52‰ $_{VPDB}$ for the Bathonian. The data revealed a constant source of CO_2 from the Aalenian to the Bathonian and a slight increase in the $\delta^{18}O$ level. The pore water in the Aalenian, from which the sideroplesite crystallized, was slightly depleted in the ^{18}O isotope compared to the pore water in the Bajocian and Bathonian.

The rhombohedral crystals of sideroplesite and pistomesite were formed at a later stage of diagenesis, which was supported by the isotope data (Table S5) and the homogenization temperature of fluid inclusions in the range of 62.0–110.0 °C [29] from the Węglany borehole. These minerals precipitated from pore water (from approximately −5.00 to +3.50‰ $_{VSMOW}$) more enriched in the ^{18}O isotope compared to water from which the early diagenetic sideroplesite precipitated, probably as a result of internal sediment-water reactions, due to sediment burial [120].

The microscopic studies have shown that calcite crystallized after sideroplesite. The $\delta^{13}C$ values indicated that carbon originated from organic matter [121]. To estimate the $\delta^{18}O$ value of pore water from which the calcite precipitated, a temperature of below 50 °C was assumed, which is indicated by the predominance of single-phase inclusions in its crystals [122]. With this assumption, the values of the $\delta^{18}O_{SMOW}$ of pore water were obtained in a range from −1.11 to +1.86‰ $_{VSMOW}$ [123].

The microscopic observations showed that ankerite was also formed at a later stage of diagenesis after sideroplesite. The $\delta^{13}C$ values indicated the origin of carbon in the tested ankerite cements generally from the decomposition of organic matter during the burial process [124]. The analysis of the fluid inclusions in ankerite demonstrated the homogenization temperature of the inclusions of about 168 °C. By assuming this level of ankerite crystallization temperature, we obtain the $\delta^{18}O_{VSMOW}$ values of pore water of about +5.00‰ $_{VSMOW}$ [125].

5.3. Diagenetic Processes

Among the diagenetic processes that affect the formation of sideritic rocks, cementation played the most important role. The dominant carbonate mineral is sideroplesite enriched with calcium and, less frequently, pistomesite. Sideroplesite is most often represented by individuals of micrite-, microspar-, and spar-sized, while pistomesite is spar-sized. In places, rhombohedral varieties of sideroplesite and pistomesite were observed, most often in sideritic sandstones and clayey-sandy siderites. The rhombohedral crystals are often zonedd, and their central part is usually richer in iron than the external part. Significant amounts of calcite and ankerite are found as the carbonate cement in sandstones and sideritic coquinas. Calcite occurs in the sideritic rocks in the southern part of the study area, while ankerite is predominantly in the northern part. Microscopic observations demonstrated that sideroplesite crystallized prior to pistomesite, calcite, and ankerite (Figure 5E–G and Table S2). The habit of sideroplesite crystals depends on the type of sideritic rock. The clayey siderites are dominated by anhedral or subhedral crystals (Figure 3A), which is probably related to the low primary porosity of the sediments. In the sandy siderites, the crystals are usually larger and better crystallized; some of them are euhedral (Figure 5D–F). This is due to the larger diameter of pores in the intergranular space, which facilitated the circulation of solutions. Among the consequences of this is, inter alia, the zonal structure of sideroplesite and pistomesite rhombohedrons that continued their development also at a later stage of diagenesis. The habit of carbonate minerals could also be controlled by the oxidation-reduction conditions of the early diagenetic environment. Carbonate cementation is also visible in the form of void fills in skeletal elements, e.g., in serpulid tubes (Figure 5H).

In addition to the carbonate cementation, authigenic vermiform kaolinite and berthierine were also observed. The cementation processes also included pyrite crystallization, locally significant, which proved the lack of oxygenation of the sediments.

Compared to the cementation, the effects of other diagenetic processes are less pronounced. Compaction is a common process in buried sediments; however, its signs are difficult to recognize in the clayey siderites. In places, the effects of compaction are the bending of mica flakes or the flattening of ooids. Mechanical compaction is better visible in sandstones, being manifested by a closer packing of detrital materials, grain fracturing, deformation of clay-mud laminae, and reduction of the primary porosity. The effects of mechanical compaction are also visible in the coquinas (Figure 5H), where dense packing of detrital materials, fracturing of skeletal elements of fossils, and flattening or crushing of ooids are observed.

The dissolution process effects are poorly visible in the sideritic rocks. The analyzed siderites locally show corrosion on the surface of quartz grains, mainly in carbonate-cemented sandstones.

Diagenetic replacement is among a large group of metasomatic processes. The effects of replacement of the previously formed rock's components by the later ones indicate that they are related to a later stage of diagenesis. In places, replacement of primary calcite by ankerite (Figure 5A), sideroplesite or phosphates is observed in bioclasts. Some berthierine ooids are partly or even completely replaced by ankerite (Figure 5C), calcite, sideroplesite, pistomesite (Figure 3F,G), and pyrite (Figure 5C); the plant detritus is often pyritized. Partial replacement of feldspar grains by sideroplesite is also observed.

Alteration effects are expressed mainly by the transformation of berthierine into kaolinite (Figure 3H). This phenomenon is best visible in ooids. Muscovite flakes, partially transformed into kaolinite, are also observed. Similar to the alteration processes are neomorphism phenomena. In the sideritic rocks, we can observe the effects of both degradational neomorphism, which are expressed by the micritization of bioclasts (probably due to the activity of microorganisms), and aggradational neomorphism, expressed by recrystallization of carbonate minerals.

Diagenetic processes also include the fracture filling. This process took place probably at a later stage of diagenesis or during uplift of the deposits. Numerous small fractures in the sideritic rocks were gradually filled with carbonate minerals and sometimes with pyrite. The fillings of veinlets often show a complex mineral composition.

5.4. Origin of Siderite

Eo-, meso-, and telodiagenesis have been distinguished in the history of diagenesis of Middle Jurassic sideritic rocks [30].

Eodiagenesis involves processes controlled by pore solutions. They were being gradually acidified due to the decomposition of some minerals and the alteration of organic matter. The main factor controlling the earliest diagenetic processes is the activity of microorganisms that decompose organic matter contained in the sediment. This stage is strongly related to sedimentary conditions. During eodiagenesis, cementation is the most strongly developed diagenetic process.

The earliest authigenic component in sideritic rocks is berthierine [28]. It occurs in the form of both clay cement (mainly in sandstones and sideritic conglomerates) and ooids. Berthierine ooids belong, according to the Kearsley [126] nomenclature, to class B and represent a kind of coated grains formed directly by diagenetic crystallization from a solution or a gel. Berthierine crystallizes at a temperature of 25–45 °C [127] under suboxic conditions at places where iron-containing fresh water and seawater mix. Berthierine, which forms in the early history of diagenesis, is chemically and structurally unstable. This means that it alters into chamosite at a temperature of about 70 °C as a result of the recrystallization process [128]. The transformation of berthierine into chamosite is a dissolution–precipitation reaction in a closed or partially closed system [129].

The main authigenic mineral in sideritic rocks is sideroplesite, locally siderite. These minerals form in a hypoxic aquatic environment at a low concentration of dissolved sulfates, in sediments rich in reactive iron-containing minerals [116,130]. Under freshwater inflow conditions, methanogenic bacteria transform organic matter to produce CO_2 and

CH_4 [131]. If CH_4 results in an increase in pH, then siderite will precipitate first at the elevated quantity of Fe^{2+}, the amount of which may increase in the absence of H_2S [132]. Clay and sulfide minerals supplied into sedimentary basins from land are considered the most common sources of iron [133,134]. According to Narębski [135], iron is also supplied in the form of colloidal suspension of $Fe(OH)_3$, and the dissolution of this compound takes place as a result of the action of CO_2-rich waters under conditions of fermentation of organic residues on the seabed. Sideroplesites that occur in the Middle Jurassic sideritic rocks are characterized by high contents of $MgCO_3$ (most often about 10 mol%) and $CaCO_3$ (commonly about 8 mol%) and a small content of $MnCO_3$ (usually about 1 mol%), indicating, according to Mozley [136], their precipitation from seawater.

Kaolinite crystallizes locally in an acidic environment [137] under conditions of significant role of meteoric waters.

Early diagenetic minerals also include pyrite (anoxic conditions). This mineral in a massive form replaces the original material of the skeleton and/or fills voids in it. However, being in the form of euhedral crystals or framboids, it fills free spaces in the rock. The type of pyritization is dependent on the concentration of dissolved iron and sulfur in the sediment and the dissolution rate of the organic material [36]. According to Sawłowicz [138], framboidal pyrite most often forms as a result of activity of bacteria present in sediments that are relatively rich in organic components.

Other eodiagenetic processes include mechanical compaction, the effects of which are visible in sandstones and coquinas in the form of tightly packed detrital material, grain fractures, or deformation of clay laminae and mica plates. Moreover, berthierine is being altered into kaolinite and replaced by sideroplestite and pyrite. In bivalve shells, secondary phosphates have also been found.

Mesodiagenesis is a long-lasting stage of transformation of sediments under conditions of increasing burial in the face of increasing mechanical compaction and dissolution under pressure. In clay siderites, which are compact and poorly permeable to formation solutions, this stage is poorly marked. In contrast, in porous sandstones, carbonate minerals precipitated as a result of the active circulation of fluids. They were filling intergranular pores and voids in bioclasts, created due to the decomposition of soft parts of organisms. Among the diagenetic processes, cementation was strongly marked.

During mesodiagenesis, the development of rhombohedral sideroplesite individuals and the formation of pistomesite continued. Crystals of these minerals commonly show a zonal structure with a significant magnesium enrichment in their outer parts, compared to the central part. The tested pistomesite is characterized by a high $MgCO_3$ content, often exceeding 20 mol% (Table S2). Magnesium for the sidederoplesite and pistomesite may have been sourced from formation water [139] or from kerogen during the sediment burial process [140]. Next, calcite and ankerite crystallized from carbonate minerals, filling the voids after the crystallization of sideroplesite and pistomesite.

An important mesodiagenetic process was metasomatic replacement. Bioclasts that were originally composed of calcite or aragonite [114] now have some skeletal elements composed of ankerite or sideroplesite. The effects of this process often blur the internal structure of bioclasts. Replacement processes have severely affected berthierine ooids. Thin sections reveal various stages of their replacement by carbonate minerals (sideroplesite, pistomesite, calcite, and ankerite) that penetrated into these grains from the outside. Many ooids have been partially replaced; in this case, their concentric structure is retained, and others have been completely replaced, most often with no signs of ordered internal structure.

During mesodiagenesis, multiple faint fracturing occurred in Jurassic rocks. Sandstones and siderites contain minute veinlets filled with calcite, ankerite, sideroplesite, and pyrite.

Telodiagenesis of the Jurassic rocks was associated with tectonic inversion of the Mid-Polish Trough in the Late Cretaceous [141]. During that period, numerous fractures appeared and there was an increased activity of pore solutions with the chemical com-

position of meteoric waters. An inflow of deep groundwater of hydrothermal origin to the analyzed Jurassic deposits cannot be ruled out. The occurrence of mineralized veins cutting through Jurassic rocks was described by Wojciechowski and Ziomek [142].

Telodiagenesis was manifested probably by partial oxidation of iron in sideroplesite concretions and layers, which was expressed by their impregnation with brown iron hydroxides. Meteoric waters could also affect the process of transforming berthierine into kaolinite.

5.5. Environment and Sideritic Rocks

Most of the studied sideritic rocks (clayey siderites and sideritic sandstones) are associated with the deposits that accumulated in the transition zone between the normal and storm wave bases and in the lower and middle shoreface in the Early and Late Bajocian and Early and Middle Bathonian. Few types of sideritic rocks are associated with the deposits formed in deeper parts of the marine basin (offshore zone) in the Late Bajocian (Mołdawa, Omięcin XI/2) and Late Aalenian (Zalesie Antoniowskie). Moreover, sideritic rocks were also commonly deposited within tide-dominated estuaries within a mud flat (Lower Aalenian) and a bayhead delta (Bathonian-Callovian). Single occurrences of siderites were also observed in carbonate ramp limestones (Upper Bathonian-Callovian) and in sandstones of fluvial origin (Lower Aalenian).

The analysis of the chemical compositions of the main carbonate mineral of sideritic rocks (sideroplesite) showed some differences depending on the environment in which they crystallized (Table S2). The highest $MgCO_3$ content (>1 mol% on average) is observed in sideroplesite from the lower and middle shoreface and mud flat zones within the tide-dominated estuary. For the transition and fluvial zones, the average $MgCO_3$ contents are 6.2 and 8.0 mol%, respectively. The lowest $CaCO_3$ value (2.7 mol% on average) was found in sideroplesite from the estuarine mud flat. It is greater in other environments and amounts to about 9.0 mol%. The average $MnCO_3$ content usually does not exceed 1 mol% in the transition zone, shoreface, and fluvial environments, while, in the estuary, it is 2.8 mol%. The average $FeCO_3$ content is highest (83.3 mol%) in the transition zone, while it is lowest (79.0 mol%) in the shoreface zone.

No relationship was found between the values of carbon isotope determinations in sideroplesite and the environmental conditions it crystallized. The average values of $\delta^{13}C$ in individual environments are similar to each other (Table S5). In the offshore, transition, shoreface, estuary (bayhead delta), estuary (mud flat), and fluvial zones, these are −7.17, −7.84, −9.41, −7.39, 5.10, and −7.34‰$_{VPDB}$, respectively. This proves the same carbon source and the formation of sideroplesite in the microbial methanogenesis zone. In the case of average $\delta^{18}O$ values in sideroplesite, there are slight differences between the environments. In the offshore, transition, shoreface, estuary (bayhead delta), estuary (mud flat), and fluvial zones, these are −3.58, −0.70, −0.26, −1.5, −3.59, and +0.50‰$_{VPDB}$, respectively. These data indicate that sideroplesite crystallized from pore water of average values of $\delta^{18}O$‰$_{VSMOW}$: −6.68 (offshore), −3.68 (transition zone), −3.02 (shoreface), −4.60 (bay-head delta), −6.73 (mud flat), and −2.51 (fluvial zone). The pore water values prove the presence of both seawater and meteoric water at different proportions in a given environment.

6. Conclusions

(1) The Lower Aalenian deposits were accumulated in a zone extending very close to the shore, probably in the outer and central parts of a tide-dominated estuary. Siderite horizons of this age are associated with fine-grained deposits that formed in the mud-flats, marginal zones of the estuary in close proximity to salt marshes.

(2) Deposition of the Upper Aalenian and the lowermost Bajocian deposits was related to a poorly oxygenated offshore environment in a vast and shallow epeirogenic sea. The upper Lower Bajocian deposits were accumulated in the transition zone between the shoreface and offshore zones, located between the storm and normal wave bases,

and then above the normal wave base in the lower shoreface environment. Siderites appear in them only in the form of small concretions.

(3) A sedimentological analysis of the Upper Bajocian and Lower-Middle Bathonian deposits showed that they are composed of several coarsening-upward cycles interpreted as prograding cycles related to a gradual shallowing of the sea. The origin of the lower members of the cycles is related to the offshore environment and/or to the transition zone between the normal and storm wave bases. The upper members were deposited in the lower and middle shoreface and, locally, also in the upper shoreface. The numerous siderite interbeds and concretions, as well as sideritization of sandstones, found in fine-grained deposits of this age are clearly related to the transition and lower shoreface zones. In the Mołdawa and Władysław boreholes, the upper section of the Middle Bathonian should be associated with the estuarine environment (the zone of sand bars and sand flat within a bayhead delta, a mud flat).

(4) The youngest rocks, Upper Bathonian-Callovian in age, were deposited in well-oxygenated environments of the upper shoreface (subtidal and intertidal zones), tide-dominated estuary, and middle and outer carbonate ramp. These rocks are barren of siderites.

(5) The Middle Jurassic sideritic rocks are most often represented by clayey siderites, which also include muddy and sandy varieties and siderite sandstones. There are also local occurrences of coquinas, claystones, mudstones, and siderite conglomerates. Most of the sideritic rocks were deposited in the transition and (lower and middle) shoreface zones.

(6) The main component of sideritic rocks is sideroplesite that was formed during early diagenesis under hypoxia conditions, in the zone of microbial methanogenesis. The isotopic composition of oxygen in sideroplesite indicates its crystallization from sea waters with the participation of meteoric waters at various proportions in a given environment.

(7) The sideroplesites that formed during early diagenesis are characterized by different crystal sizes. In general, sideroplesite is commonly very finely crystalline in clayey siderites, while, in sandy siderites and sideritic sandstones, the crystals often exceed 20 μm in size. Locally, in larger sideroplesite crystals, their outer parts are enriched in magnesium compared to the central zone. Crystallization of sideroplesite in the sediment was linked with an increasing inflow of magnesium (up to 22.5 mol% $MgCO_3$) as the sediment burial proceeded, which is clearly visible in the crystals that show a zonal structure. The proportion of calcium in sideroplesite is variable, within the range of 0.4–16.1-mol% $CaCO_3$. A relatively high content of magnesium and calcium in sideroplesite may indicate its marine origin.

(8) An important component of sideritic rocks is berthierine. It occurs mainly as the cement in sandstones and sideritic coquinas and in the form of berthierine ooids. Berthierine in ooids is often replaced by carbonates: ankerite, calcite, sideroplesite, pistomesite, and pyrite, as well as altered into kaolinite.

(9) Sideritic rocks contain varying amounts of bioclasts. These are fragments of bivalves, brachiopods, gastropods, foraminifera, echinoderms, and serpulid tubes. The primary components of bioclasts underwent the processes of replacement, especially by sideroplesite and ankerite. Pyrite and phosphates are also observed within the bioclasts.

(10) The rich mineral composition observed in the sideritic sandstones may be a result of the persistent porosity of the sandstones, which facilitates the circulation of pore fluids. The sequence of carbonate minerals composing the sandstone cements is as follows: sideroplesite I (micrite) → sideroplesite II (microspar and spar) → pistomesite → calcite → ankerite. Calcite is found in sideritic rocks in the southern part of the study area, while ankerite is present mostly in the northern part.

(11) The action of diagenetic processes of cementation, compaction, replacement and alteration within the Middle Jurassic deposits was most intense during the eo- and mesodiagenesis. The most important process in the formation of siderites was cementation.

(12) Sedimentological analysis shows that most of the studied siderites were formed in a low-oxygenated marine environment, mainly in the transition zone between the normal and storm wave bases and in the lower shoreface zone. On the other hand, the Lower Aalenian siderites were formed in a very shallow water environment, probably in the marginal parts of the estuary (mud flat) near salt marshes. The results of petrographic, mineralogical and geochemical studies indicate the origin of sideritic rocks mainly in the marine environment, with the participation of meteoric water.

(13) There are slight differences in the chemical composition of sideroplesite depending on the environment it crystallized. The highest average content of $FeCO_3$ (83.3 mol%) is in the transition zone; of $MgCO_3$ (>11 mol%) in the shoreface and estuary; of $CaCO_3$ (9 mol%) in the transition, shoreface, and fluvial zones; and of $MnCO_3$ (2.8 mol%) in the estuary.

(14) There is no correlation between the values of carbon isotope determinations in sideroplesite and the environmental conditions of its crystallization. The average values of $\delta^{13}C$ in the individual environments are similar and are about −7.00 ‰$_{VPDB}$, which proves the same carbon source. Slight differences are visible in the case of average values of $\delta^{18}O$ in sideroplesite. They vary from −3.58 ‰$_{VPDB}$ in the offshore zone to + 0.50 ‰$_{VPDB}$ in the fluvial zone, which indicates the presence of both sea water and meteoric water at different proportions, depending on the environment.

Supplementary Materials: The following are available online at https://www.mdpi.com/article/10.3390/min11121353/s1: Table S1: Composition of clayey siderites (vol. %)*; Table S2: Chemical composition of carbonates from microprobe analyses; Table S3: Composition of sideritic sandstones (vol. %)*; Table S4: Composition of sideritic coquinas (vol. %)*; Table S5: Isotopic ratios of carbon and oxygen in carbonate cements (values of $\delta^{18}O_{VSMOW}$ of crystalline water for sideroplesite precipitated in temperature 20 °C).

Author Contributions: Conceptualization, A.K., A.M. and A.F.-O.; methodology, A.K., A.F.-O. and M.K.; software, A.K. and A.F.-O.; validation, A.K. and A.F.-O.; formal analysis, A.K. and A.F.-O.; investigation, A.K., A.F.-O. and M.K.; resources, A.K., A.F.-O., M.K. and A.M.; writing—original draft preparation, A.K. and A.F.-O.; writing—review and editing, A.K. and A.F.-O.; visualization, A.K. and A.F.-O.; and supervision, A.K. and A.F.-O. All authors have read and agreed to the published version of the manuscript.

Funding: This research received no external funding.

Acknowledgments: Two ananymus reviewers are thanked for their comments and suggestions that help the authors improve the manuscript. The XRD analysis was performed by W. Narkiewicz and the SEM examination by L. Giro and E. Starnawska. S. Hałas and the team are acknowledged for the oxygen and carbon isotopic analyses. This paper is a part of projects No. N N307 330339 financed by the Ministry of Science and Higher Education and No. 61.2201.0604.00.0 of the Polish Geological Institute–National Research Institute.

Conflicts of Interest: The authors declare no conflict of interest.

References

1. Kuźniar, C. O rudach żelaznych okolic Chlewisk. *Posiedz. Nauk. Państw. Inst. Geol.* **1924**, *8*, 1–2. (In Polish)
2. Kuźniar, C. O rudach żelaznych okolic Stąporkowa. *Posiedz. Nauk. Państw. Inst. Geol.* **1925**, *10*, 6–7. (In Polish)
3. Kuźniar, C. Złoże rud żelaznych oolitowych w Parczewie. *Spraw. Państw. Inst. Geol.* **1928**, *4*, 710–763. (In Polish)
4. Jaskólski, S. Złoża oolitowych rud żelaznych obszaru częstochowskiego. *Rocz. Pol. Tow. Geol.* **1928**, *4*, 1–91. (In Polish)
5. Jaskólski, S.; Sawicka-Ekiert, E. Badania petrograficzne.InBadania geologiczne iłów rudonośnych jury krakowsko-wieluńskiej, obszar między Krzepicami a Wręczycą. *Biul. Inst. Geol.* **1955**, *1*, 5–46. (In Polish)
6. Znosko, J. Uplift of the Kłodawa salt dome during the Jurassic, and its influence upon the formation of the sideritic lumachel rocks. *Kwart. Geol.* **1957**, *1*, 90–105. (In Polish)
7. Znosko, J. Górny wezul jury łęczyckiej. *Biul. Inst. Geol.* **1958**, *126*, 477–507. (In Polish)
8. Różycki, S.Z. Badania geologiczne i roboty poszukiwawcze w roku 1938 w strefie występowania jury na północnym i wschodnim obrzeżeniu Gór Świętokrzyskich. *Państw. Inst. Geol. Biul.* **1939**, *15*, 43–58. (In Polish)
9. Różycki, S.Z. Parkinsonie, garantiany i strenocerasy z doggeru obrzeżenia Gór Świętokrzyskich i ich znaczenie stratygraficzne. *Acta Geol. Polonica* **1955**, *5*, 305–341. (In Polish)

10. Karaszewski, W. *Sprawozdanie z Badań z Okolicy Inowłodza nad Pilicą*; Archive Materials; Narodowe Archiwum Geologiczne Polish Geolological Institute, NRI: Warsaw, Poland, 1947. (In Polish)
11. Cieśla, E. Aalenian beds in bore-hole Brudzewice (Central Poland). *Kwart Geol.* **1957**, *1*, 440–448. (In Polish)
12. Cieśla, E. Nowe dane o przebiegu północnej części antykliny Inowłodzkiej. *Prz. Geol.* **1958**, *3*, 125. (In Polish)
13. Daniec, J. The Dogger of the middle part of the northeastern surrounding cover of the Święty Krzyż Mountains. *Biul. Inst. Geol.* **1963**, *168*, 37–85. (In Polish)
14. Daniec, J. Middle Jurassic. In *The Stratigraphy of the Mesozoic in the Góry Świętokrzyskie*; Prace Instytutu Geologicznego; Pożaryski, W., Ed.; Państwowy Instytut Geologiczny: Warsaw, Poland, 1970; Volume 56, pp. 99–133. (In Polish)
15. Turnau-Morawska, M. Petrographic character of the ironstone of the Vesulian in the Łęczyca region. *Biul. Inst. Geol.* **1961**, *172*, 5–69. (In Polish with English Summary)
16. Dadlez, J. Niektóre wyniki badań nad wykształceniem i rudonośnością wezulu w okolicach Kamienia Pomorskiego. *Biul. Inst. Geol.* **1963**, *168*, 5–36. (In Polish)
17. Dadlez, J. *Wyniki Badań Rudonośności Osadów Wezulu w Rejonie Niczonowa*; Archive Materials; Narodowe Archiwum Geologiczne Polish Geolological Institute, NRI: Warsaw, Poland, 1964. (In Polish)
18. Ekiert, E. *Opracowanie Petrograficzne Rud Liasowych Środkowej Części Antyklinorium Pomorskiego*; Archive Materials; Narodowe Archiwum Geologiczne Polish Geolological Institute NRI: Warsaw, Poland, 1964. (In Polish)
19. Maliszewska, A. (Ed.) Middle Jurassic. In *Diagenesis of the Upper Permian and Mesozoic Deposits of the Kujawy Region (Central Poland)*; Prace Instytutu Geologicznego; Państwowy Instytut Geologiczny: Warsaw, Poland, 1999; Volume 167, pp. 78–93. (In Polish)
20. Maliszewska, A.; Kozłowska, A.; Kuberska, M. Origin od Middle Jurassic siderite rocks from Central Poland. *Vol. Jurass.* **2006**, *4*, 95–96.
21. Maliszewska, A.; Kozłowska, A.; Kuberska, M. *Petrologia Jurajskich Skał Syderytowych na Niżu Polskim*; Archive materials; Archiwum Geologiczne MNiSW: Warsaw, Poland, 2007. (In Polish)
22. Maliszewska, A.; Kozłowska, A.; Kuberska, M. *Syderyty Jurajskie Kujaw i Wielkopolski: Studium Petrologiczne*; Archive materials; Narodowe Archiwum Geologiczne Polish Geolological Institute, NRI: Warsaw, Poland, 2007. (In Polish)
23. Maliszewska, A.; Kozłowska, A.; Kuberska, M. The Middle Jurassic sideritic rocks of the Kujawy area—Petrological study. *Prz. Geol.* **2018**, *66*, 118–129. (In Polish with English Summary)
24. Kozłowska, A.; Feldman-Olszewska, A.; Kuberska, M.; Maliszewska, A.; Złonkiewicz, Z. *Skały Syderytowe Jury Środkowej w Północnym Obrzeżeniu Gór Świętokrzyskich a Warunki Ich Sedymentacji i Diagenezy*; Archive materials; Narodowe Archiwum Geologiczne Polish Geolological Institute NRI: Warsaw, Poland, 2008. (In Polish)
25. Kozłowska, A.; Feldman-Olszewska, A.; Kuberska, M.; Maliszewska, A. Sedimentary environments and diagenesis of the Middle Jurassic siderites in the Noth Margin of the Holy Cross Mountains, Poland. In Proceedings of the 28th Meeting of Sedimentology (IAS 2011), Book of Abstracts, Zaragoza, Spain, 5–8 July 2011; p. 522.
26. Kozłowska, A.; Feldman-Olszewska, A.; Jarmołowicz-Szulc, K.; Kuberska, M.; Maliszewska, A. *Diageneza Syderytowych Rud Żelaza Jury Środkowej z Północnego Obrzeżenia Gór Świętokrzyskich i Obszaru Częstochowsko-Wieluńskiego*; Archive Materials; Archiwum Geologiczne MniSW: Warsaw, Poland, 2013. (In Polish)
27. Kozłowska, A. Diageneza skał syderytowych jury środkowej na południe od Tomaszowa Mazowieckiego. In Proceedings of the Przewodnik Wycieczek terenowych, Abstrakty i Artykuły, Konferencja Jurassica XI, Jurajskie Utwory Synkliny Tomaszowskiej, Spała, Poland, 9–11 October 2014; Volume 50. (In Polish)
28. Kozłowska, A.; Maliszewska, A. Berthieryn in the Middle Jurassic sideritic rocks from southern Poland. *Geol. Quart.* **2015**, *59*, 551–564.
29. Jarmołowicz-Szulc, K.; Kozłowska, A. Temperature and isotopic relations in carbonate minerals in the Middle Jurassic sideritic rocks of central and southern Poland. *Geol. Quart.* **2016**, *60*, 881–892. [CrossRef]
30. Kozłowska, A. Instrumental methods applied in the investigations of carbonate minerals in the Middle Jurassic sideritic rocks with respect to diagenetic processes. *Biul. PIG* **2019**, *474*, 31–42. [CrossRef]
31. Kozłowska, A.; Feldman-Olszewska, A.; Jarmołowicz-Szulc, K.; Kuberska, M.; Maliszewska, A. The Middle Jurassic siderites from Częstochowa-Wieluń area, southern Poland. In Proceedings of the 34 IGC International Geological Congres, Brisbane, Australia, 5–10 August 2012; p. 1526.
32. Majewski, W. Middle Jurassic concretions from Częstochowa (Poland) as indicator of sedimentation rates. *Acta Geol. Pol.* **2000**, *50*, 431–439.
33. Zatoń, M.; Marynowski, L. Konzentrat-Lagerstätte—Type carbonate concretions from the upper-most Bajocian (Middle Jurassic) of the Częstochowa area, SW Poland. *Geol. Quart.* **2004**, *48*, 339–350.
34. Zatoń, M.; Marynowski, L.; Bzowska, G. Hiatus concretions from the ore-bearing clays of the Cracow-Częstochowa Upland (Polish Jura). *Prz. Geol.* **2006**, *54*, 131–138. (In Polish with English Summary)
35. Szczepanik, P.; Witkowska, M.; Sawłowicz, Z. Geochemistry of Middle Jurassic mudstones (Kraków-Częstochowa area, southern Poland): Interpretation of the depositional redox conditions. *Geol. Quart.* **2007**, *54*, 57–66.
36. Geld, P.; Kaim, A.; Leonowicz, P.; Boczarowski, A.; Dudek, T.; Kędzierski, M.; Rees, J.; Smoleń, J.; Szczepaniak, P.; Sztainer, P.; et al. Palaeoenvironmental reconstruction of Bathonian (Middle Jurassic) ore-bearing clays at Gnaszyn, Kraków-Silesia Homocline, Poland. *Acta Geol. Pol.* **2012**, *62*, 463–484.

37. Leonowicz, P. Sedimentology and ichnology of Bathonian (Middle Jurassic) ore-bearing clays at Gnaszyn, Kraków–Silesia Homocline, Poland. *Acta Geol. Pol.* **2012**, *62*, 281–296. [CrossRef]
38. Leonowicz, P. The significance of mudstone fabric combined with palaeoecological evidence in determing sedimentary processes—An example from the Middle Jurassic of southern Poland. *Geol. Quart.* **2013**, *57*, 243–260.
39. Leonowicz, P. Storm-influenced deposition and cyclicity in a shallow-marine mudstone succession–example from the Middle Jurassic ore-bearing clays of the Polish Jura (southern Poland). *Geol. Quart.* **2015**, *59*, 325–344. [CrossRef]
40. Leonowicz, P. Nearshore transgresive black shale from the Middle Jurassic shallow-marine succession from southern Poland. *Facies* **2016**, *62*, 16. [CrossRef]
41. Khim, B.-K.; Coi, K.-S.; Park, Y.-A.; Oh, J.-K. Occurrence of authigenic siderites in the Early Holocene coastal deposit in the west coast of Korea: An indicator of depositional environment. *Geosci. J.* **1999**, *3*, 163–170. [CrossRef]
42. Akinlotan, O. Sideritic ironstones as indicators of depositional environments in the Weald Basin (Early Cretaceous) SE England. *Geol. Mag.* **2017**, *156*, 533–546. [CrossRef]
43. Campbell, M.D.; Campbell, M.D. Paleoenvironmental implicatoms of selected siderite zones in the Upper Atoka Formation, Arkoma Basin, Oklahoma-Arkansas: A look back and current views on siderite genesis in a sedimentary environment. *Int. J. Earth Sci. Geol.* **2018**, *1*, 1000103.
44. Mizerski, W. Holy Cross Mountains in the Caledonian, Variscan and alpine cycles—Major problems, open questions. *Prz. Geol.* **2004**, *8*, 774–779.
45. Dadlez, R. Holy Cross Mts. area—Crustal structure, geophysical data and general geology. *Geol. Quart.* **2001**, *45*, 99–106.
46. Konon, A. Strike-slip faulting in the Kielce Unit, Holy Cross Mountains, central Poland. *Acta Geol. Pol.* **2007**, *57*, 415–441.
47. Żelaźniewicz, A.; Aleksandrowski, P.; Buła, Z.; Karnkowski, P.H.; Konon, A.; Oszczypko, N.; Ślączka, A.; Żaba, J.; Żytko, K. *Regionalizacja Tektoniczna Polski*; Komitet Nauk Geologicznych PAN: Wrocław, Poland, 2011. (In Polish)
48. Narkiewicz, M.; Dadlez, R. Geological regional subdivision of Poland: General guidelines and proposed schemes of sub-Cenozoic and sub-Permian units. *Prz. Geol.* **2008**, *56*, 391–397. (In Polish with English Summary).
49. Kutek, J. The Polish Permo-Mesozoic Rift Basin. In *Mémoires du Muséum National d'Histoire Naturelle*; Editions du Muséum: Paris, France, 2001; Volume 186, pp. 213–236.
50. Złonkiewicz, Z. Evolution of the Miechów Depression basin in the Jurassic as a result of regional tectonical changes. *Prz. Geol.* **2006**, *54*, 534–540. (In Polish with English Summary)
51. Dadlez, R.; Marek, S.; Pokorski, J. (Eds.) *Palaeogeographical Atlas of the Epikontinental Permian and Mesozoic in Poland 1: 2,500,000*; Wydawnictwa Geologiczne: Warsaw, Poland, 1998.
52. Krzywiec, P. Mid-Polish Trough inversion—Seismic examples, main mechanisms, and its relationship to the Alpine-Carpathian collision. In *EGS Stephan Mueller Special Publication Series*; European Geological Society: Munich, Germany, 2002; Volume 1, pp. 233–258.
53. Marek, S.; Znosko, J. Tectonics of the Kujawy Region. *Kwart. Geol.* **1972**, *16*, 1–18. (In Polish with English Summary)
54. Pożaryski, W. *Budowa Geologiczna Polski, Tektonika, Niż Polski*; Wydawnictwa Geologiczne: Warsaw, Poland, 1974; Volume 4, p. 1. (In Polish)
55. Stupnicka, E. *Geologia Regionalna Polski*; Wydawnictwa Geologiczne: Warsaw, Poland, 1989. (In Polish)
56. Dadlez, R.; Marek, S.; Pokorski, J. *Mapa Geologiczna Polski bez Utworów Kenozoiku (Skala 1:1,000,000)*; Państwowy Instytut Geologiczny: Warsaw, Poland, 2000.
57. Mader, A.; Mniszków, I.G. *Profile Głębokich Otworów Wiertniczych Państwowego Instytutu Geologicznego*; Państwowy Instytut Geologiczny Państwowy Instytut Badawczy: Warsaw, Poland, 2021, in press. (In Polish)
58. Farrell, K.M.; Harris, W.B.; Mallinson, D.J.; Culver, S.J.; Riggs, S.R.; Pierson, J.; Self-Trail, J.M.; Alautier, J.C. Standardizing Texture and Facies Codes for a Process-Based Classification of Clastic Sediment and Rock. *J. Sediment. Res.* **2012**, *82*, 364–378. [CrossRef]
59. Zieliński, T.; Pisarska-Jamroży, M. Which features of deposits should be included in a code and which not? *Prz. Geol.* **2012**, *60*, 387–397. (In Polish with English Summary)
60. Reineck, H.E.; Singh, I.B. *Depositional Sedimentary Environments*; Springer: Berlin/Heidelberg, Germany; New York, NY, USA, 1975.
61. Walker, R.G. *Facies Models*; Geoscience Canada Reprint 1; Geological Association of Canada Publications: St. John's, NL, Canada, 1984.
62. Einsele, G. *Sedimentary Basins*; Springer: Berlin/Heidelberg, Germany, 1992; p. 628.
63. MacEachern, J.A.; Pemberton, S.G. Ichnological aspects of Cretaceous shoreface successions and shoreface variability in the Western Interior Seaway of North America. In *Application of Ichnology to Petroleum Exploration, SEPM Core Workshop*; Pemberton, G.S., Ed.; Society for Sedimentary Geology: Tulsa, OK, USA, 1992; Volume 17, pp. 57–84.
64. Pemberton, S.G.; Van Wagoner, J.; Wach, G.D. Ichnofacies of wave-dominated shoreline. In *Application of Ichnology to Petroleum Exploration, SEPM Core Workshop*; Pemberton, G.S., Ed.; Society for Sedimentary Geology: Tulsa, OK, USA, 1992; Volume 17, pp. 339–382.
65. Pemberton, S.G.; Spila, M.; Pulham, A.J.; Saunders, T.; Maceachern, J.A.; Robbins, D.; Sinclair, I.K. *Ichnology and Sedimentology of Shallow to Marginal Marine Systems: Ben Nevis and Avalon Reservoirs, Jeanne d'Arc Basin*; Short Course Notes; Geological Association of Canada: St. John's, NL, Canada, 2001; Volume 15, p. 343.
66. Reading, H.G. *Sedimentary Environments: Processes, Facies and Stratigraphy*; Blackwell Science Ltd.: Hoboken, NJ, USA, 1996.

67. Feldman-Olszewska, A. Środowiska Sedymentacji w Jurze Środkowej Kujaw. Ph.D. Thesis, Polish Geological Institute-National Research Institute, Warsaw, Poland, 2005. (In Polish)
68. Feldman-Olszewska, A. Sedimentary environments of the Middle Jurassic epicontinental deposits from the central part of the Polish Basin (Kuiavian Region). In *Volumina Jurassica IV, Abstracts of Talks and Posters 86 Presented during the 7th International Congerss on the Jurassic System, Kraków, Poland, 6–18 September 2006*; Polish Geological Institute: Warsaw, Poland, 2006.
69. Feldman-Olszewska, A. Analiza sedymentologiczna utworów środkowej jury. In *Ciechocinek IG 2, Profile Głębokich Otworów Wiertniczych Państwowego Instytutu Geologiczneg*; Feldman-Olszewska, A., Ed.; Państwowy Instytut Geologiczny—Państwowy Instytut Badawczy: Warsaw, Poland, 2007; Volume 117, pp. 54–65. (In Polish)
70. Feldman-Olszewska, A. Wyniki badań sedymentologicznych utworów jury środkowej w otworze wiertniczym Brześć Kujawski IG 2. In *Brześć Kujawski IG 1, IG 2, IG 3, Profile Głębokich Otworów Wiertniczych Państwowego Instytutu Geologiczneg*; Feldman-Olszewska, A., Ed.; Państwowy Instytut Geologiczny—Państwowy Instytut Badawczy: Warsaw, Poland, 2008; Volume 125, pp. 151–154. (In Polish)
71. Feldman-Olszewska, A. Wyniki badań sedymentologicznych utworów jury środkowej w otworze wiertniczym Brześć Kujawski IG 3. In *Brześć Kujawski IG 1, IG 2, IG 3, Profile Głębokich Otworów Wiertniczych Państwowego Instytutu Geologiczneg*; Feldman-Olszewska, A., Ed.; Państwowy Instytut Geologiczny—Państwowy Instytut Badawczy: Warsaw, Poland, 2008; Volume 125, pp. 154–157. (In Polish)
72. Feldman-Olszewska, A. Trace fossils in the Middle Jurassic epicontinental deposits from the central part of the Polish Basin (Kuiavian region). In Proceedings of the Second International Congress on Ichnology, Cracow, Poland, 29 August–8 September 2008; Abstract book and the intra-congress field trip guidebook. 2008; pp. 38–39.
73. Feldman-Olszewska, A. Wyniki badań sedymentologicznych utworów jury środkowej w wierceniu Wojszyce IG 1a. In *Wojszyce IG 1/1a, Wojszyce IG 3, Wojszyce IG 4, Brześć Kujawski IG 1, IG 2, IG 3, Profile Głębokich Otworów Wiertniczych Państwowego Instytutu Geologiczneg*; Feldman-Olszewska, A., Ed.; Państwowy Instytut Geologiczny—Państwowy Instytut Badawczy: Warsaw, Poland, 2012; Volume 137, pp. 149–152. (In Polish)
74. Feldman-Olszewska, A. Wyniki badań sedymentologicznych utworów jury środkowej w wierceniu Wojszyce IG 3. In *Wojszyce IG 1/1a, Wojszyce IG 3, Wojszyce IG 4, Profile Głębokich Otworów Wiertniczych Państwowego Instytutu Geologiczneg*; Feldman-Olszewska, A., Ed.; Państwowy Instytut Geologiczny—Państwowy Instytut Badawczy: Warsaw, Poland, 2012; Volume 137, pp. 152–158.(In Polish)
75. Feldman-Olszewska, A. Wyniki badań sedymentologicznych utworów jury środkowej w wierceniu Wojszyce IG 4. In *Wojszyce IG 1/1a, Wojszyce IG 3, Wojszyce IG 4, Profile Głębokich Otworów Wiertniczych Państwowego Instytutu Geologiczneg*; Feldman-Olszewska, A., Ed.; Państwowy Instytut Geologiczny—Państwowy Instytut Badawczy: Warsaw, Poland, 2012; Volume 137, pp. 158–166. (In Polish)
76. Dayczak-Calikowska, K.; Kopik, J. Jura środkowa. In *Budowa Geologiczna Polski, Mezozoik*; Sokołowski, S., Ed.; Wydawnictwa Geologiczne: Warsaw, Poland, 1973; Volume 2, pp. 237–325. (In Polish)
77. Dayczak-Calikowska, K. Aalen i dolny bajos w południowej części Kujaw. *Kwart. Geol.* **1976**, *20*, 751–763. (In Polish)
78. Dayczak-Calikowska, K.; Moryc, W. Evolution of sedimentary basin and palaeotectonics of the Middle Jurassic in Poland. *Kwart. Geol.* **1988**, *32*, 117–135. (In Polish with English Summary).
79. Feldman-Olszewska, A. Early Aalenian–Callovian Palaeogeography. In *Palaeogeographical Atlas of the Epikontinental Permian and Mesozoic in Poland 1: 2,500,000*; Dadlez, R., Marek, S., Pokorski, J., Eds.; Wydawnictwa Geologiczne: Warsaw, Poland, 1998; pp. 37–48.
80. McCrea, J.M. On the isotopic geochemistry of carbonates and a paleotemperature scale. *J. Chem. Phys.* **1950**, *18*, 849–857. [CrossRef]
81. Al-Aasm, I.S.; Taylor, B.E.; South, B. Stable isotope analysis of multiple carbonate samples using selective acid extraction. *Chem. Geol.* **1990**, *80*, 119–125. [CrossRef]
82. Hałas, S. An automatic inlet system with pneumatic changeover valves for isotope ratio mass spectrometer. *J. Phys. E Sci. Instrum.* **1979**, *18*, 417–420.
83. Hałas, S.; Skorzyński, Z. An unexpensive device for digital measurements of isotopic ratios. *J. Phys. E Sci. Instrum.* **1980**, *13*, 346–349. [CrossRef]
84. Durakiewicz, T.; Hałas, S. Triple collector system for isotope ratio mass spectrometer. *IF UMCS Repor.* **1994**, 131–132.
85. Durakiewicz, T. Electron emission controller with pulsed heating of filament. *Int. J. Mass. Spectrom. Ion Process.* **1996**, *156*, 31–40. [CrossRef]
86. Bolewski, A. *Mineralogia Szczegółowa*; Wydawnictwa Geologiczne: Warsaw, Poland, 1982. (In Polish)
87. Folk, R.L. Practical petrographic classification of limestones. *AAPG* **1959**, *43*, 1–38.
88. Allen, G.P.; Posamentier, H.W. Sequence stratigraphy and facies model of an incisted valley fill: The Gironde estuary, France. *J. Sediment. Petrol.* **1993**, *63*, 378–391.
89. Nichols, M.M.; Johnson, G.H.; Peebles, P.C. Modern sediments and facies model for a microtidal coast plain estuary, the James Estuary, Virginia. *J. Sediment. Petrol.* **1991**, *61*, 883–899.
90. Walker, R.G. An incisted valley in the Cardium Formation at Ricinus, Alberta: Reinterpretation as an estuary fill. In *Sedimentary Facies Analysis: A Tribute to the Research and Teaching of Harold, G. Reading*; Special Publication International Association of Sedimentologists Series; Plint, A.G., Ed.; John Wiley & Sons: Hoboken, NJ, USA, 1995; Volume 22, pp. 47–74.

91. Terwind, J.H.J. Litho-facies of inshore estuarine and tidal-inlet deposits. *Geol. Mijnbow* **1971**, *50*, 515–526.
92. Visser, M.J. Neap-spring cycles reflected in Holocene subtidal large-scale bedform deposits: A preliminary note. *Geology* **1980**, *8*, 543–546. [CrossRef]
93. Bergman, K.M. Shannon Sandstone in Hartzog draw fields (Cretaceous, Wyoming, USA) reinterpreted as lowstand shoreface deposits. *J. Sediment. Res.* **1994**, *64*, 184–201.
94. Seilacher, A. Bathymetry of trace fossils. *Mar. Geol.* **1967**, *5*, 413–428. [CrossRef]
95. Dalrymple, R.W.; Zaitlin, B.A.; Boyd, R. Estuarine facies models: Conceptual basis and stratigraphic implications. *J. Sediment. Petrol.* **1992**, *62*, 1130–1146. [CrossRef]
96. Clifton, H.E. Estuarine deposits. In *Sandstone Depositional Environments*; Schole, P.A., Spearing, D., Eds.; American Association of Petroleum Geologists: Tulsa, OK, USA, 1982; Volume 31, pp. 179–189.
97. Pieńkowski, G.; Michael, E.; Schudack, M.E.; Bosák, P.; Enay, R.; Feldman-Olszewska, A.; Golonka, J.; Gutowski, J.; Herngreen, G.F.W.; Jordan, P.; et al. *The Geology of Central Europe, Mesozoic and Cenozoic*; McCann, T., Ed.; The Geologfical Society: London, UK, 2008; Volume 2, pp. 823–922.
98. Feldman-Olszewska, A. Depositional architecture of the Polish epicontinental Middle Jurassic basin. *Geol. Quat.* **1997**, *41*, 491–508.
99. Wignal, P.B. *Black Shales*; Oxford University Press: Oxford, UK, 1994; p. 127.
100. Reineck, H.E.; Wünderlich, F. Classification and origin of flasher and lenticular bedding. *Sedimentology* **1968**, *11*, 99–104. [CrossRef]
101. Gradziński, R.; Kostecka, A.; Radomski, A.; Unrug, R. *Zarys Sedymentologii*; Wydawnictwa Geologiczne: Warszawa, Poland, 1986. (In Polish)
102. Dott, R.H.; Bourgeois, J. Hummocky stratification: Significance of its variable bedding sequences. *Geol. Soc. Am. Bull.* **1982**, *93*, 663–680. [CrossRef]
103. Lott, G.; Wong, T.; Dusar, M.; Andsbjerg, J.; Monnig, E.; Feldman-Olszewska, A.; Verreussel, R. Jurassic. In *Petroleum Geological Atlas of the Southern Permian Basin Area*; Doornenbal, H., Stevenson, A., Eds.; EAGE Publications: Houten, The Netherlands, 2010; pp. 173–193.
104. Swift, D.J.P. Fluid and sediment dynamics on continental shelves. In *Shelf Sands and Sandstone Reservoirs*; SEPM Short Course Notes; Tillman, R.W., Swift, D.J.P., Walker, R.G., Eds.; Society for Sedimentary Geology: Tulsa, OK, USA, 1985; Volume 13, pp. 47–134.
105. Walker, R.G. Cardium Formation 4. Review of facies and depositional processes in the southern foothils and plains, Alberta, Canada. In *Shelf Sands and Sandstone Reservoirs*; SEPM Short Course Notes; Tillman, R.W., Swift, D.J.P., Walker, R.G., Eds.; Society for Sedimentary Geology: Tulsa, OK, USA, 1985; Volume 13, pp. 353–402.
106. Walker, R.G. Comparison of shelf environments and deep basin turbidite systems. In *Shelf Sands and Sandstone Reservoirs*; SEPM Short Course Notes; Tillman, R.W., Swift, D.J.P., Walker, R.G., Eds.; Society for Sedimentary Geology: Tulsa, OK, USA, 1985; Volume 13, pp. 465–502.
107. Walker, R.G. Cardium and Viking sandstone cores. In *Shelf Sands and Sandstone Reservoirs*; SEPM Short Course Notes; Tillman, R.W., Swift, D.J.P., Walker, R.G., Eds.; Society for Sedimentary Geology: Tulsa, OK, USA, 1985; Volume 13, pp. 645–676.
108. Fruit, D.J.; Elmore, R.D. Tide and storm-dominated sand ridges on a muddy shelf: Cottage Grove Sandstone (Upper Pennsylvanian), Northwestern Oklahoma. *AAPG Bull.* **1988**, *72*, 1200–1211.
109. Porębski, S.J. Świebodzice succession (Upper Dewonian-Lowest Carboniferous Western Sudetes): A prograding, mass-flow dominated fan-delta complex. *Geol. Sudet.* **1981**, *16*, 101–194. (In Polish with English Summary)
110. Leckie, D.; Walker, R.G. Storm-and tide-dominated shorelines in Cretaceous Moosebar-Lower Gates interval—Outcrop equivalents of deep basin gas trap in Western Canada. *AAPG Bull.* **1982**, *66*, 138–157.
111. Leckie, D. Tidally influenced, transgressive shelf sediments in the Viking Formation, Caroline, Alberta. *Bull. Can. Pet. Geol.* **1986**, *34*, 111–125.
112. Cheel, R.J.; Leckie, D.A. Hummocky cross-stratification. In *Sedimentology Review*; Wright, V.P., Ed.; Blackwell Scientific Publications: Hoboken, NJ, USA, 1993; pp. 103–122.
113. Worden, R.H.; Griffiths, J.; Wooldridge, L.J.; Utley, J.E.P.; Lawan, A.Y.; Muhammed, D.D.; Simon, N.; Armitage, P.J. Chlorite in sandstones. *Earth Sci. Rev.* **2020**, *204*, 103105. [CrossRef]
114. Flügel, E. *Microfacies of Carbonate Rocks*; Springer: Berlin/Heidelberg, Germany, 2010; p. 984.
115. Irvin, H.; Curtis, C.; Coleman, M. Isotopic evidence for source of diagenetic carbonates formed during burial of organic-rich sediments. *Nature* **1977**, *269*, 209–213.
116. Morad, S. (Ed.) *Carbonate Cementation in Sandstone: Distribution Patterns and Geochemical Evolution*; Special Publicaiton International Association of Sedimentologists; Wiley-Blackwell: Hobooken, NJ, USA, 1998; Volume 26, pp. 1–26.
117. Gruszczyński, T. Chemistry of Jurassic seas and its bearing on the existing organic life. *Acta Geol. Pol.* **1998**, *48*, 1–30.
118. Coleman, M.L.; Feldman-Olszewska, A.; Gaździcka, E.; Gruszczyński, M. Sekwencje depozycyjne, a zapis izotopowo-geochemiczny wybranych odcinków czasowych jury środkowej i górnej w centralnej części Niżu Polskiego. In *Materiały Konferencyjne, VI Krajowe Spotkanie Sedymentologów, Lewin Kłodzki*; WIND: Wrocław, Poland, 1997; pp. 4–6. (In Polish)
119. Carothers, W.W.; Adami, L.H.; Rosenbauer, R.J. Experimental oxygen isotope fractional between siderite-water and phosphoric acid liberated CO_2–siderite. *Geochim. Cosmochim. Acta* **1988**, *52*, 2445–2450. [CrossRef]
120. Mc Kay, J.L.; Longstafee, F.J.; Plint, A.G. Early diagenesis and its relationship to depositional environment and relative sea-level fluctuations (Upper Cretaceous) Marshybank Formation, Alberta and British Columbia. *Sedymentology* **1995**, *42*, 161–190. [CrossRef]

121. Baker, J.C. Diagenesis and reservoir quality of the Aldebaran Sandstone, Denison Trough, east-central Queensland, Australia. *Sedimentology* **1991**, *38*, 819–838. [CrossRef]
122. Goldstein, R.H.; Reynolds, T.J. Systematic of fluid inclusions in diagenetic minerals. *SEMP Short Course* **1994**, *31*, 199.
123. Friedman, I.; O'Neil, J. Compilation of stable isotope fractionation factors of geochemical interst. In *Data of Geochemistry*; Fleischer, M., Ed.; Professional Paper; U.S. Geological Survey: Reston, VA, USA, 1977; Volume 440-K, pp. 1–12.
124. Ayalon, A.; Longstaffe, F.J. Stable isotope evidence for the origin of diagenetic carbonate minerals from Lower Jurassic Inmar Formation, Southern Israel. *Sedimentology* **1995**, *42*, 147–160. [CrossRef]
125. Dutton, S.P.; Land, L.S. Meteoric burial diagenesis of pensylvanian arkosic sandstones, Southwestern Anadarko Basin, Texas. *AAPG Bull.* **1985**, *69*, 22–38.
126. Kearsley, A.T. Iron-rich ooids, their mineralogy and microfabric: Clues to their origin and evolution. In *Phanerozoic Ironstones*; Geological Society Special Publications; Young, T.P., Taylor, W.E.G., Eds.; The Geological Society: London, UK, 1989; Volume 46, pp. 141–164.
127. Hornibrook, E.R.C.; Longstaffe, F.J. Berthierine from the Lower Cretaceous Clearwater Formation, Alberta, Canada. *Clays Clay Miner.* **1996**, *44*, 1–21. [CrossRef]
128. Jahren, J.S.; Aagaard, P. Compositional variations in diagenetic chlorites and illites and relationships with formation-water chemistry. *Clay Miner.* **1989**, *24*, 157–170. [CrossRef]
129. Aagard, P.; Jahren, J.S.; Harstad, A.O.; Nilsen, O.; Ramm, M. Formation of grain-coating chlorite in sandstones. Laboratory synthesize vs. natural occurrences. *Clay Miner.* **2000**, *35*, 261–269. [CrossRef]
130. Browne, G.H.; Kingston, D.M. Early diagenetic spherulitic siderites from Pensylvanian palaeosols in the Boss Point Formation, Maritime Canada. *Sedimentology* **1993**, *40*, 467–474. [CrossRef]
131. Claypool, G.E.; Kaplan, I.R. The origin and distribution of methane in marine sediments. In *Natural Gases in Marine Sediments*; Kaplan, I.R., Ed.; Marine Science; Springer: Boston, MA, USA, 1974; Volume 3, pp. 97–139.
132. Hugget, J.; Dennis, P.; Gale, A. Geochemistry of early siderite cements from the Eocene succession of Whitecliff Bay, Hampshire Basin, U.K. *J. Sediment. Res.* **2000**, *70*, 1107–1117. [CrossRef]
133. Pearson, M.J. Geochemistry of the Hepworth Carboniferous sediment sequence and origin of the diagenetic iron minerals and concretions. *Geochim. Cosmochim. Acta* **1979**, *43*, 927–941. [CrossRef]
134. Price, G.D.; Sellwood, B.W. "Warm" palaeotemperatures from high Late Jurassic palaeolatitudes (Falkland Plateau): Ecological, environmental or diagenetic controls? *Palaeogeogr. Palaeoclimatol. Palaeocol.* **1997**, *129*, 315–327. [CrossRef]
135. Narębski, W. Mineralogia i geochemiczne warunki genezy tzw. syderytów fliszu karpackiego. *Arch. Miner.* **1958**, *21*, 5–100. (In Polish)
136. Mozley, P.S. Relation between depositional environment and the elemental composition of early diagenetic siderite. *Geology* **1989**, *17*, 704–706. [CrossRef]
137. Osborne, M.; Haszeldine, R.S.; Fallick, A.E. Variation in kaolinite morphology with growth temperature in isotopically mixed pore-fluids, Brent Group: UK North Sea. *Clay Miner.* **1994**, *29*, 591–608. [CrossRef]
138. Sawłowicz, Z. Framboids: From their origin to application. *Pr. Mineral.* **2000**, *88*, 1–70.
139. Morad, S.; Ben Ismail, H.N.; De Ros, L.F.; Al-Aasm, I.S.; Sherrhini, N.E. Diagenesis and formation water chemistry of Triassic reservoir sandstones from Southern Tunisia. *Sedimentology* **1994**, *41*, 1253–1272. [CrossRef]
140. Desborough, G.A. A biogenic–chemical stratified lake model for the origin of oil shale of the Green River Formation: On alternative to the playa–lake model. *Geol. Soc. Am. Bull.* **1978**, *89*, 961–971. [CrossRef]
141. Dadlez, R.; Marek, S. Structural style of the Zechstein–Mesozoic complex in some areas of the Polish Lowland. *Kwart. Geol.* **1969**, *13*, 3. (In Polish with English Summary)
142. Wojciechowski, J.; Ziomek, J. On sphalerite occurence in siderites of ore-bearing series at Łęczyca (Central Poland). *Prz. Geol.* **1966**, *7*, 319–321. (In Polish with English Summary)